Petroleum Science 22 (2025) 5239–5257

Contents lists available at ScienceDirect

Petroleum Science

journal homepage: www.keaipublishing.com/en/journals/petroleum-science

Original Paper

Optimal fit clearance of control valve considering energy consumption based on loosely coupled fluid-solid interaction

Ning Xu [a,d], Shi-Min Zhang [a], De-Li Jia [b], Kun Tian [c], Yan-Hong Wei [c], Xiao-Xiao Zhu [a,**], Peichun Amy Tsai [d,*]

[a] College of Mechanical and Transportation Engineering, China University of Petroleum (Beijing), Beijing, 102249, China
[b] Research Institute of Petroleum Exploration and Development, PetroChina, Beijing, 100083, China
[c] Guizhou Aerospace Kaishan Petroleum Instrument Co., Ltd., China Aerospace Science and Industry Corporation Limited, Guiyang, 550025, Guizhou, China
[d] Department of Mechanical Engineering, University of Alberta, Edmonton, Alberta T6G 1H9, Canada

ARTICLE INFO

Article history:
Received 21 September 2024
Received in revised form
15 January 2025
Accepted 23 September 2025
Available online 27 September 2025

Edited by Teng Zhu

Keywords:
Energy consumption
Control valve
Fit clearance
Loosely coupled fluid-structure interaction
Contact friction
Optimization

ABSTRACT

The wireless intelligent water distributor is an emerging technology increasingly applied in oilfields to enhance oil recovery. Although the system has many advantages, the high energy consumption of its integrated control valve hinders its adoption in long-term applications. However, existing studies have not sufficiently captured the mechanical characteristics of forces acting on the spool, particularly under the influence of multiple coupled factors, such as fit clearance, deflection, and fluid-structure interaction, which limit the ability to accurately assess energy consumption. To address this gap, this study develops a comprehensive energy consumption model of the control valve, specifically addressing the design of fit clearance, a critical factor influencing energy efficiency. Utilizing a loosely coupled fluid–structure interaction algorithm, we established a mechanical model of the spool to investigate the fluid-solid interaction mechanisms within the fit clearance. For the first time, the effects of contact friction on energy consumption are incorporated. An optimization algorithm was then applied to determine the optimal fit clearance by balancing low friction and minimal leakage. The validity of our numerical model was confirmed through comparison with both theoretical and experimental results. Our results demonstrate that the fit clearance has a pronounced impact on the valve's energy usage: the total maximum energy consumption for one full stroke with a 0.05 mm clearance is 3.33% higher than with a 0.25 mm clearance. When the spool is independently driven, this value is 7.21%. The optimal fit clearance is determined to be 0.127 mm. These results can improve the overall performance and extend the service life of intelligent water distributors. The findings and models developed in this study provide essential theoretical support and practical strategies for optimizing control valve energy consumption.
© 2025 The Authors. Publishing services by Elsevier B.V. on behalf of KeAi Communications Co. Ltd. This is an open access article under the CC BY-NC-ND license (http://creativecommons.org/licenses/by-nc-nd/4.0/).

1. Introduction

Wireless water distributors have emerged as cost-effective, easily operated devices with significant potential for large-scale application in layered water injection, improving oil recovery efficiency (Liu et al., 2023). These devices integrate flowmeters, manometers, communication modules, and control valves, utilizing pressure wave or flow wave communication technology for wireless communication with surface systems (Wang et al., 2020). Despite their advantages, large-scale deployment is challenged by energy limitations due to battery capacity and self-discharge. As a result, strict management of usage time and power consumption is essential to ensure functionality beyond three years (Liu et al., 2023).

Among the components of wireless water distributors, the energy consumption of the control valve is particularly critical. These valves not only generate fluid pulse signals for wireless communication but also regulate flow in real time (Ming et al., 2023). By 2020, 144, 104 injection wells were in operation, and

* Corresponding author.
** Corresponding author.
E-mail addresses: x.zhu@cup.edu.cn (X.-X. Zhu), peichun@ualberta.ca (P.A. Tsai).
Peer review under the responsibility of China University of Petroleum (Beijing).

https://doi.org/10.1016/j.petsci.2025.09.037
1995-8226/© 2025 The Authors. Publishing services by Elsevier B.V. on behalf of KeAi Communications Co. Ltd. This is an open access article under the CC BY-NC-ND license (http://creativecommons.org/licenses/by-nc-nd/4.0/).

the frequency of flow adjustments far exceeded the number of wells (Liu et al., 2017). As high water-cut reservoirs continue to develop, both the number of wells and the frequency of adjustments are expected to rise, increasing control valve energy consumption (Lei et al., 2019). Moreover, with global policies aiming to reduce energy usage in oil and gas development (Zheng et al., 2022), low-power control valve design has become a key research focus (Zhao and Liu, 2020).

Previous studies have demonstrated potential improvements in valve energy efficiency. For example, Simic and Herakovic (2015) found that modifying the spool geometry and valve housing significantly reduces hydrodynamic forces, achieving a 10% reduction in energy consumption at a 100 Hz switching frequency. Amirante et al. (2014) improved spool performance by modifying the conical surface at the spool's end, reducing the maximum driving force by 8% compared to standard valves. Chen et al. (2023a) proposed reducing steady-state hydrodynamic forces by adjusting the spool's shoulder angle. Wu et al. (2024) applied an improved rectangular groove structure to reduce spool deformation and friction forces. Additionally, Zhang et al. (2022) showed that refining the spool profile modifies internal flow, lowering energy consumption. Asim et al. (2019) minimized energy loss by optimizing local flow parameters based on geometry.

Despite these advances, most studies have focused on improving the spool structures to reduce flow forces and energy consumption, while overlooking the frictional effects arising from deformation under fluid-structure interaction. Existing studies offer baseline energy estimates but lack precision in calculating friction and axial forces on the spool, which are critical for accurately assessing energy use during motion conversion. Therefore, research is needed to thoroughly evaluate and optimize valve energy consumption, particularly considering frictional forces.

Measuring frictional characteristics experimentally is challenging due to the small magnitude of variables such as fit clearance, which is often comparable to experimental errors. Moreover, optimizing fit clearance requires extensive and costly testing procedures. Existing theories mainly address axial clearance flow and are insufficient to explain complex gap flow distributions, particularly those involving lateral outlets, as considered in this study (Li and Wu, 2020). The impact of high-pressure fluid on the spool generates frictional forces due to the combined effects of fluid flow and solid deformation. These interactions are difficult to visualize experimentally, and existing theoretical models fail to adequately describe their complexity. As a result, two-way fluid-structure interaction (FSI) simulations present a promising approach to capture frictional effects and accurately evaluate the control valve's energy consumption. To ensure reliable calculations, a comprehensive model must incorporate all critical components, including the sealing system, bearings assembly, and motion conversion mechanism. Based on this foundation, a robust mechanical analysis model is essential to precisely calculate the spool's mechanical behavior, effectively capturing both frictional and axial forces.

Constructing a mechanical analysis model of the spool requires a clear understanding of the influencing factors. Prior studies have shown that fit clearance plays a critical role in determining the spool's force characteristics (Li and Wu, 2020; Xu et al., 2024). Current designs typically prioritize control accuracy and reliability, leaving considerable room for energy efficiency optimization (Liu et al., 2016; Kong et al., 2018; Xu et al., 2019). During the fit clearance design process, factors such as random spool deflection and leakage must be carefully addressed (Xu et al., 2024). A small fit clearance often causes the spool to contact the valve body during deflection, leading to deformation and increased contact friction, which elevates energy consumption (Hong and Kim, 2016). Conversely, a large fit clearance may result in substantial leakage and reduced flow regulation capability (Li and Wu, 2020). The design must also ensure that the valve spool does not stick due to excessive contact friction (Luo et al., 2022). The interdependent and conflicting nature of these objectives, minimizing friction, leakage, and energy consumption, presents a complex optimization challenge. Optimization algorithms can assist in identifying the fit clearance that best balances these competing goals, thereby achieving an optimal configuration under minimized objective values (Liu et al., 2021). Currently, control valve designs tend to favor larger fit clearances (greater than 50 μm) to reduce the risk of spool sticking. For these larger clearances, it is generally assumed that thermal deformation of the spool, pressure-induced radial deformation, and fluid property variations are negligible (Xu et al., 2024).

Several researchers have developed models to address these complexities (Zhang et al., 2020; Chen et al., 2023b; Qian et al., 2023; Yin et al., 2023). However, many of these models fail to capture the critical solid-solid contact behavior between the spool and the valve body. Although numerous studies on contact friction have investigated its fundamental mechanisms, such as the mechanical characteristics at contact points, frictional wear, and lubrication characteristics (Zhu et al., 2019; Zhang et al., 2021; Kang et al., 2022; Wang et al., 2024). Nevertheless, these investigations are primarily confined to microscopic contact surfaces. As a result, they offer limited insights into macroscopic friction forces encountered in real-world applications, where solid-solid contact due to spool deflection, external loads, and material deformation is unavoidable (Li and Wu, 2020; Zhao et al., 2023). Neglecting these friction effects may result in inaccurate evaluations of spool mechanical behavior and leakage characteristics, potentially leading to design failures associated with increased energy consumption. At present, there is a notable lack of research that systematically examines the mechanisms of fluid-solid interaction within the fit clearance, especially under multi-factor coupling conditions involving spool deflection, deformation and clearance variation. The interplay of these factors can significantly amplify frictional resistance, thereby compromising the energy efficiency of the system.

Existing models, therefore, have yet to investigate the underlying mechanisms of fluid-solid interaction within the fit clearance, making it difficult to accurately predict energy consumption under realistic operating conditions where high friction is prevalent. To address this gap, we propose the application of a loosely coupled FSI algorithm as a viable solution. This algorithm alternates between solving the fluid and solid domains and adapts by remeshing the fluid domain near the solid-solid contact area after each iteration. This approach not only captures complex contact forces with high fidelity but also maintains low computational cost (Souli et al., 2000). Furthermore, the loosely coupled FSI method has been effectively applied to simulate large deformations and strong nonlinearities in other domains (Guo et al., 2017; Bucelli et al., 2023). However, to date, no reported applications of this method exist in the context of control valves. In contrast, traditional FSI algorithms require solving the fully coupled model at each time step, which involves high algorithmic complexity and strict dynamic mesh constraints to maintain solution accuracy. By implementing the loosely coupled FSI approach, energy consumption in control valves can be evaluated with high precision, while significantly reducing computational complexity. This enables the development of more energy-efficient valve designs without sacrificing accuracy.

This study aims to develop a comprehensive energy consumption model, along with a detailed mechanical analysis model of the spool, to enable accurate evaluation of control valve energy

usage. The primary objective is to optimize the fit clearance in control valves to enhance their energy efficiency. Using a loosely coupled fluid-structure interaction (FSI) algorithm, we constructed a high-fidelity mechanical model that accounts for spool deflection and contact deformation. This model is used to investigate the fluid-solid coupling mechanisms within the fit clearance and to capture solid-solid contact behaviors under realistic operating conditions. The proposed models allow for the evaluation of maximum energy consumption, leakage, and spool friction forces. An optimization algorithm is then employed to determine the optimal fit clearance. This work addresses a critical gap in current energy consumption modeling by incorporating complex fluid-structure interactions, an area particularly underexplored in the context of wireless water distributor control valves. The models and optimization strategies developed herein provide valuable tools for improving stratified water injection efficiency, reducing operational energy consumption, and extending the service life of wireless intelligent water distributors in oilfield applications.

2. Control valve structure

Developing a comprehensive energy consumption model for a control valve first requires a clear understanding of the dimensions and functional characteristics of each component. Based on the physical model of the control valve depicted in Fig. 1, Fig. 2 provides a visual representation highlighting the key components and their respective functions during valve operation: (1) Coupling and sliding screw: At the core of the control valve's operation is a coupling that connects the driving motor to a sliding screw. This assembly is critical as it converts the rotational motion from the motor into linear motion required for spool actuation. (2) Bearing system: Surrounding the sliding screw is a robust bearing system that provides radial support, ensuring stable and smooth operation. (3) Sealing system: This system is designed to prevent water ingress, thereby protecting the electronic components and the driving motor from water damage. It enhances valve reliability and extends service life. (4) Transitional structure: This includes a support surface and two sets of internal threads, one that engages with the external thread of the sliding screw, and another that connects directly to the spool. This configuration enables smooth spool movement within the valve body, facilitated by the support surface. (5) Fluid flow management: Fluid enters through the inlet and is regulated by the spool's throttling effect before exiting through the outlet. This flow control is central to the valve's ability to meet system requirements.

Fig. 3 illustrates the spool posture and details the structural parameters of the constructed model, which are identical to those of the actual control valve. The key geometric parameters are defined as follows:

O: Initial center of the support end face.

O_1 and O_2: Centers of support end face after deflection.

e_1 and e_2: Deflections of O_1 and O_2, respectively.

α_1 and α_2: Deflection angles of O_1 and O_2, respectively.

These parameters allow for precise control of the spool's relative position using the defined deflections and deflection angles: e_1, e_2, as well as α_1 and α_2. Additionally, key model dimensions are as follows:

Lengths: Sealing surface l_0: 5 mm. Outlet l_1: 18 mm. Support surface l_2: 13.5 mm. Spool l_3: 24 mm. Connection section l_4: 30 mm.

Inner diameters: Chamber (d_0 and d_4): 12 mm and 14 mm.

Diameters: Spool d_1: 11.8 mm. Transition section d_2: 10 mm. Support surface d_3: 14 mm. Initial fit clearance δ: 0.1 mm.

Fig. 4 shows the outlet configuration, the outlet lengths (l_5 and l_6) are specified as 4.5 mm and 13.5 mm, respectively, with a width l_7 of 7.2 mm.

3. Comprehensive energy consumption model

3.1. Loosely coupled fluid-solid interaction algorithm

Due to the spool's frequent contact with the valve body, driven by deflection and fluid forces, a two-way FSI solution is essential for detailed and accurate analysis. The traditional strongly coupled FSI algorithm establishes a proximity threshold to ensure the distance between the deformed solid and the solid boundary does not fall below a specified value. This approach effectively prevents fluid mesh splitting due to direct contact and enables simulation of contact deformation (Rao, 2003). However, it requires solving fluid-structure interactions at each time step, necessitating

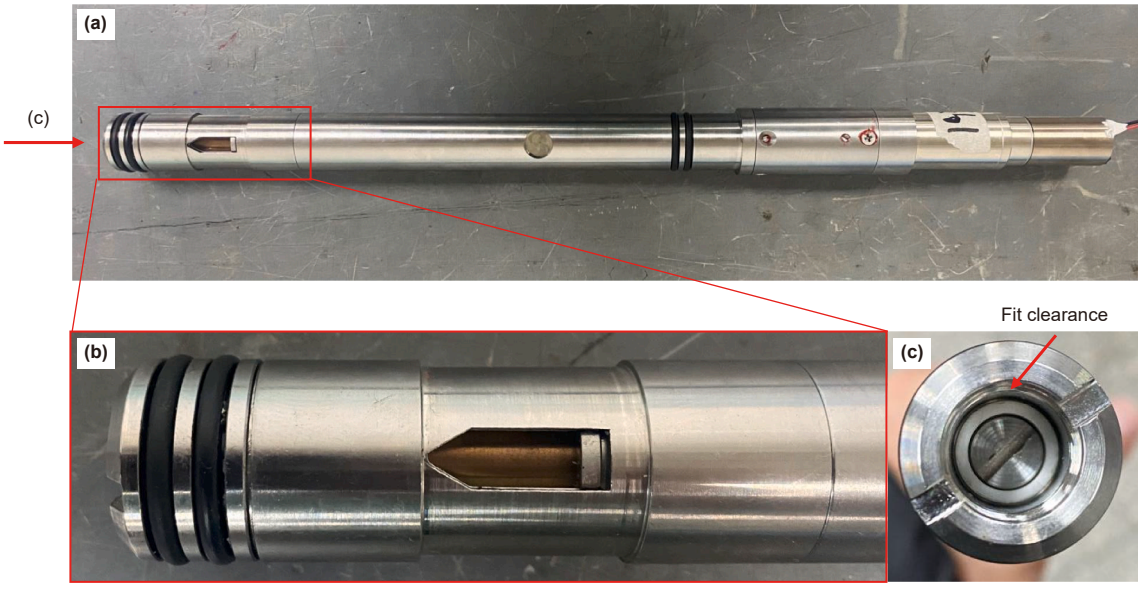

Fig. 1. Control valve physical module.

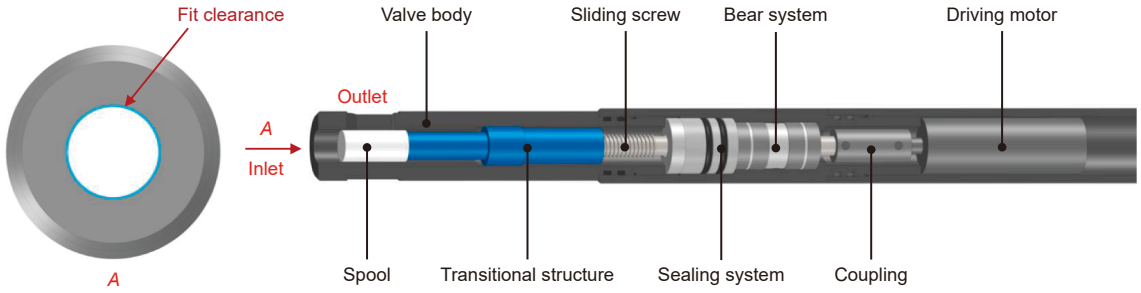

Fig. 2. Control valve configuration. The fit clearance refers to the gap between the spool and the valve body.

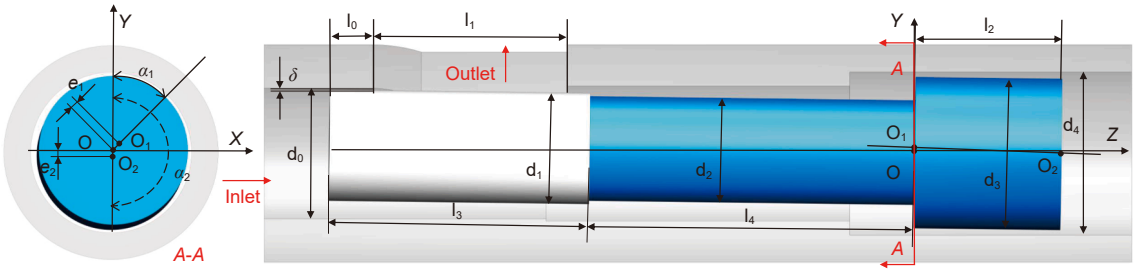

Fig. 3. Relative posture of the spool and valve.

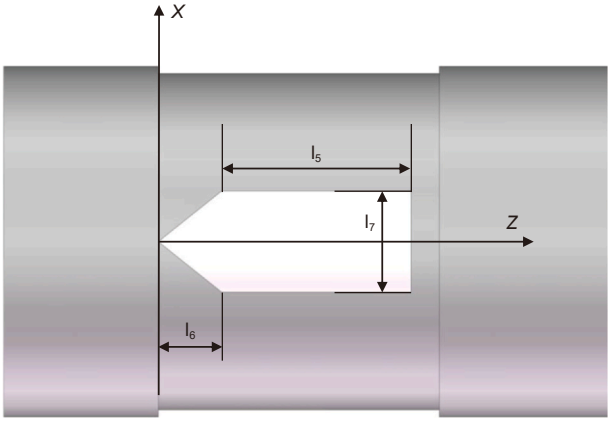

Fig. 4. Dimensions of outlet shape.

complex algorithms and stringent dynamic mesh conditions, which significantly increase computational cost and numerical complexity.

To address these challenges, this study employs a loosely coupled FSI algorithm (Farhat et al., 2006; Gigante and Vergara, 2021). This algorithm solves the fluid and solid domains alternately, allowing for bidirectional interaction between fluid pressure and spool deformation. By decoupling the fluid and solid domains, the fluid mesh is reconstructed after each iteration, avoiding mesh distortion caused by solid-solid contact and enabling accurate capture of contact friction. Loosely coupled FSI also supports more flexible time stepping, thereby accelerating the solution process, especially in quasi-static simulations. In this method, fluid and solid solvers are run independently, reducing computational time, lowering code complexity, and simplifying the interaction process. Moreover, this approach can be easily integrated with existing fluid and solid solvers without requiring extensive customization. Fig. 5(a) shows the flowchart of the loosely coupled FSI approach, illustrating the iterative processes involved in the simulation.

Modeling process:

(1) Model construction: A three-dimensional model of the control valve was created using SolidWorks software, matching the actual dimensions shown in Fig. 3. The model includes the spool and valve body as solid domains, and a separate 3D model of the fluid passage was created to define the fluid domain.

(2) Mesh generation: The constructed fluid and solid domains were imported into Integrated Computer Engineering and Manufacturing (ICEM) software, where Boolean operations were used to extract the fluid domain. At this stage, the fluid and solid domains are non-overlapping and mutually independent. The fluid domain was discretized using hexahedral meshes, as referenced in Xu et al. (2024). The spool surface was defined as the data interaction surface, while inlet and outlet sections were appropriately designated. All other surfaces were treated as walls. The solid domain was meshed using tetrahedral elements, with the spool surface set as the interaction surface and the support surfaces defined as fixed constraints. Mesh resolution for both domains was determined based on a mesh independence study, as detailed in Section 5.2.

(3) Flow field simulation: The fluid mesh was imported into Fluent software, where a steady-state approach was applied (You et al., 2021). Boundary conditions, including inlet and outlet parameters, continuous flow model, and fluid properties, are detailed in Section 5.1. Upon completion of the simulation, the pressure distribution on the spool surface was extracted and used as input for the solid domain.

(4) Structural simulation: The solid domain was analyzed using structural mechanics software. The boundary conditions including fixed constraints, initial deformation, connection methods, and material properties, are described in Section 5.1. The pressure distribution from Step 3 was applied, and the resulting spool deformation was calculated.

(5) Reconstruction of the fluid domain: The deformation results from Step 4 were exported. Since the deformation was

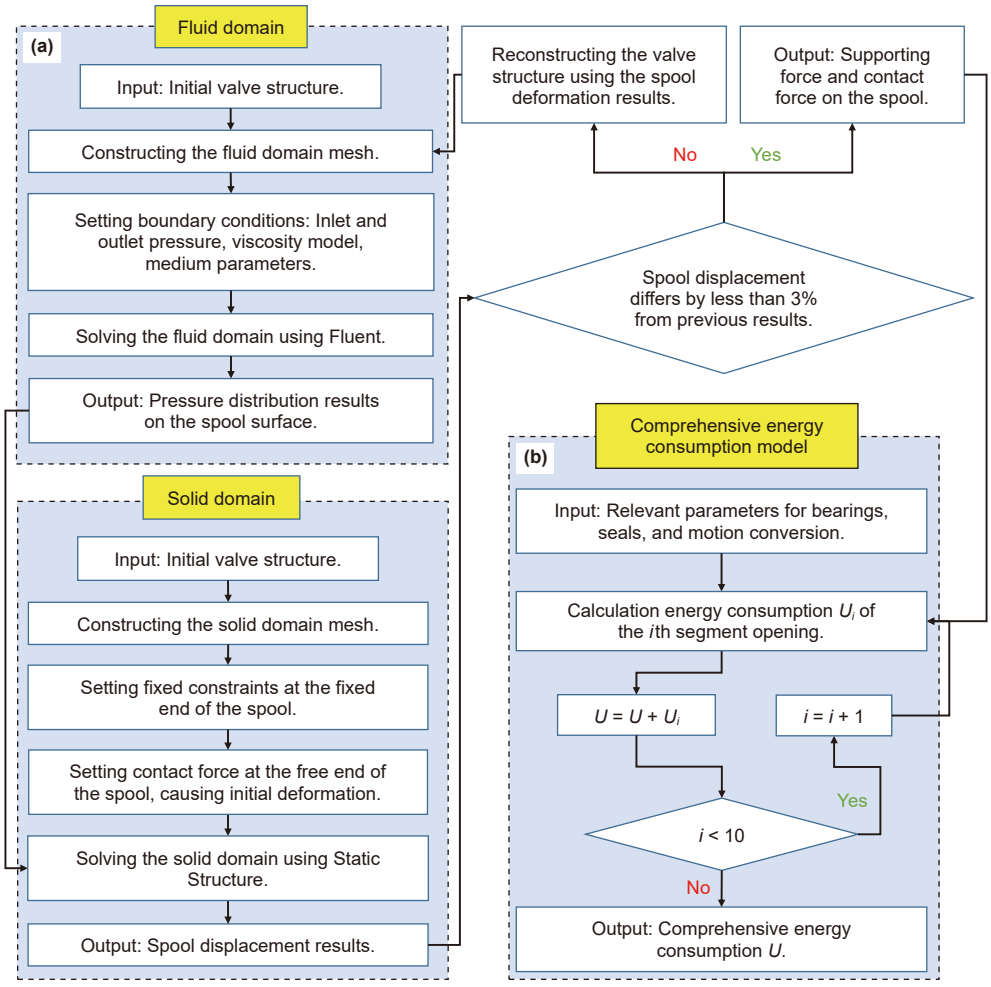

Fig. 5. Loosely coupled fluid-solid interaction flowcharts.

minor, four control points (A1–A4) were selected to characterize the spool deformation. Fig. 6 illustrates the control volume used for analyzing spool deformation. The fluid mesh fully encloses the spool but did not extend beyond the fit clearance. A new deformed 3D model of the spool was then reconstructed using the same procedure as in Step 1. Steps 2 and 3 were repeated to extract the updated pressure distribution on the spool surface.

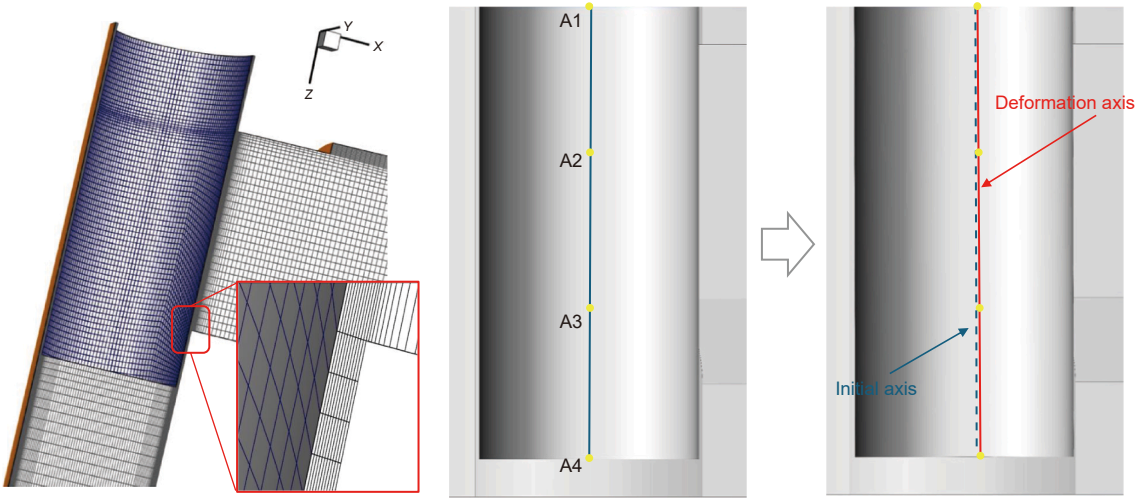

Fig. 6. Schematic of deformation driven by control points.

(6) Iterative process: The updated pressure distribution from Step 5 was reapplied to the solid domain as a boundary condition. Following Step 4, the displacement results of the control points were updated. This process was repeated until the difference between successive spool deformation results was less than 3%, indicating convergence. This iterative loop ensures that the forces exerted by the fluid on the solid and the reactive forces from the solid on the fluid are balanced, achieving equilibrium.

3.2. Comprehensive energy consumption calculations

The control valve's energy consumption primarily results from the friction torque generated by its components during rotational motion. The calculation process, illustrated in Fig. 5(b), involves evaluating the friction torque contributions from the sealing elements, bearing systems, and sliding screw, followed by a comprehensive calculation of total energy consumption over the entire valve stroke. Frictional torque from the sliding screw is determined by analyzing the axial forces acting on the spool, which arise from both fluid pressure and contact friction. To systematically capture these forces, a mechanical analysis model is developed to compute all forces acting on the spool at various valve openings, as detailed in Section 3.1.

To account for the varying force characteristics across the opening range, the finite element method (FEM) was employed to discretize the valve stroke into smaller intervals (Kudela and Matousek, 2022). For each finite element, the frictional torque exerted on the drive motor at a specific valve opening was calculated. The energy consumption for each segment is then determined and aggregated to yield the total energy consumption for the entire stroke. The detailed process is as follows:

(1) Discrete valve openings: The entire opening range is divided into ten intervals, with a representative sample opening selected from each. Due to the small interval size, the boundary conditions of the control valve were assumed to remain constant over short durations, and the spool motion was sufficiently slow to justify the quasi-steady-state assumption. Within each interval, the forces acting on the spool are treated as constant.
(2) Frictional torque calculations: The mechanical analysis model described in Section 3.1 is used to compute all relevant forces at each valve opening, including axial and contact forces, as illustrated in Fig. 5(a). The frictional force is obtained by substituting the contact force into Eqs. (21) and (22). Both the frictional and axial forces are then input into Eq. (7), to calculate the friction torque for the sliding screw. The friction torque for the sealing and bearing systems are determined using standard formulas presented in Section 4.2 (Eqs. (5)–(6)).
(3) Energy consumption calculations: For each sample opening, the energy consumption U_i is computed based on the friction torque using Eqs. (8)–(10). The total energy consumption U is then obtained by summing the individual values across all intervals. This approach enables a high-fidelity analysis of the control valve's energy use, while maintaining computational efficiency.

By employing this method, the control valve's energy consumption, including the effects of contact friction and axial forces, can be comprehensively evaluated across different valve openings, providing a precise and efficient energy assessment framework.

4. Theoretical models

4.1. Flow characteristics

The design of the fit clearance δ must strike a balance between energy consumption and leakage Q_l. Q_l reflects the degree to which the control valve deviates from its intended fluid control function and is evaluated using the following performance indicators.

The valve relative opening l represents the extent to which a valve is open, typically expressed as a percentage of its full stroke. The inherent flow characteristic function $f(l)$ describes the relationship between the relative flow rate and the valve's relative opening under a constant pressure drop. This function is crucial for analyzing the valve's flow regulation performance across different operating conditions (Ye et al., 2014) and is defined by:

$$q = \frac{Q}{Q_{\max}} = f\left(\frac{L}{L_{\max}}\right) = f(l) \tag{1}$$

where q represents the relative flow rate, Q and $Q_{\max}$ denote the flow rate at a specific opening and the maximum opening, L/min, respectively. Here, L and $L_{\max}$ are the stroke at a particular opening and the maximum opening, m, respectively.

The commonly used inherent flow characteristics are linear, equal percentage, and quick opening (Xu et al., 2024). Among these, the linear inherent flow characteristic provides a constant amplification factor and offers good sensitivity across the operating range. Therefore, it is selected as a basis for designing the fit clearance δ. The linear flow characteristic (Zhang et al., 2022) is expressed as:

$$\frac{Q}{Q_{\max}} = K\frac{L}{L_{\max}} + C \tag{2}$$

where K represents the scaling factor, and C is a constant.

Another important parameter for characterizing the valve's flow performance is the flow coefficient, C_υ (Li et al., 2024), which quantifies the valve's flow capacity at a specific opening. It is a key indicator for evaluating the valve's ability to regulate fluid flow and is calculated as:

$$C_\upsilon = \frac{Q}{N}\sqrt{\frac{\rho/\rho_0}{\Delta p}} \tag{3}$$

where N is the unit conversion coefficient, with a value of 14.42; Δp denotes the pressure difference between the inlet and outlet, bar; ρ represents the density of the working medium, kg/m^3; ρ_0 is the density of working medium at 15 °C, kg/m^3. When the flowing medium is standard-temperature water, the value of ρ/ρ_0 is 1.

4.2. Friction torque model

The motor drive torque M_z is utilized to overcome the inertia, friction, and other resistances of the load, thereby enabling rotational motion within the mechanical system and inherently consumes energy. In low-speed control valves, M_z is primarily used to overcome the friction torque and to control the valve stroke. The torque required by the driving motor M_z, which is essential for accurate energy calculations, is represented as:

$$M_z = M_b + M_s + M_p \tag{4}$$

where M_b represents the bearing friction torque, N·m; M_s denotes the sealing friction torque, N·m; and M_p signifies the sliding screw friction torque, N·m.

To ensure valve operation, motor drive must overcome M_b generated within the bearings (Ding et al., 2024), which is calculated using:

$$M_b = \frac{\mu_b F_b d_b}{2} \tag{5}$$

where μ_b is the friction coefficient of the bearings; F_b is the radial load on the bearings, N; and d_b is the inner diameter of the bearings, m.

Control valves typically employ packing seal systems, which generating resistive torque due to contact friction between the packing and the stem. This resistive torque, known as seal friction torque M_s, significantly affects both energy consumption and sealing performance, making it a crucial parameter in control valve design (Ding et al., 2024). M_s is determined by:

$$M_s = \frac{\mu_s \pi d_a^2 h p_s}{2} \tag{6}$$

where μ_s represents the friction coefficient of the sealing system, which is made of polytetrafluoroethylene (PTFE); d_a denotes the diameter of the shaft, m; h represents the length of the sealing surface, m; p_s indicates the necessary sealing pressure acting on the sealing surface, MPa.

The sliding screw converts motor torque into axial thrust, enabling the spool movement. During operation, it generates M_p due to friction at the thread contact surfaces (Xie et al., 2023). M_p is defined by:

$$M_p = \frac{d_1 F \tan(\lambda + \rho')}{2} \tag{7}$$

where d_1 is the mean diameter of the thread, m; F is the axial load of the screw drive, N; λ is the helix angle of the screw, °; ρ' is the equivalent friction angle, °.

The motor's angular displacement φ (rad) is directly related to the axial displacement x (m) of the spool. The control valve stroke can be divided into infinitesimal axial displacements, where the axial displacement of the spool within each microelement section is given by:

$$\mathrm{d}l = \frac{\mathrm{d}\varphi}{2\pi} S = \frac{\mathrm{d}\varphi}{2\pi} P\gamma \tag{8}$$

where S is the lead, m; P is the pitch, m; γ is the number of threads.

The axial movement speed v (in m/s) of the spool is directly related to the motor's rotational speed n, rev/min. The relationship between these parameters is

$$v = \frac{\omega}{2\pi} S = \frac{n}{60} S \tag{9}$$

where ω denotes the angular velocity of the motor, rad/s.

The electrical energy consumption U of a motor refers to the energy consumed over a specific period, kW· h. Due to the varying load on the spool during its stroke, the motor continuously adjusts its M_z to maintain synchronous speed. The integral expression for calculating U is given by:

$$U = Pt = \int_0^t \frac{M_z n}{9550000} \mathrm{d}t \tag{10}$$

where P is the driving power (kW) of the motor, and t is the stroke duration, h.

4.3. Mechanical analysis model

In practical applications, spool deflection can cause contact with the valve body, resulting in initial deformation. This deformation is further aggravated by fluid dynamic forces, leading to cumulative structural deformation. Assuming that the boundary conditions remain unchanged, the spool is considered to be in a state of force equilibrium. At this point, the support surface of the spool temporarily maintains fixed contact with the valve body, while the spool end face behaves as a free end. Therefore, cantilever beam theory can be used to describe the deformation behavior of the spool (Beléndez et al., 2002). The deflection w_B (m) of the center of the spool end face under the applied contact force F_n (N) is given by:

$$w_B = \frac{F_n L^3}{3EI} \tag{11}$$

$$I = \frac{\pi d_2^4}{64} \tag{12}$$

where L is the beam length, m; E is the material's modulus of elasticity, Pa; and I is the inertia moment of the beam's cross-section, mm^4.

The deflection angle θ_B (in °) at the spool end face's center is calculated by Beléndez et al. (2002):

$$\theta_B = \frac{F_n L^2}{3EI} \tag{13}$$

The fluid force acting on the spool is treated as a distributed load. Based on the direction of action, it can be divided into an axial force F_z and a radial force F_l, N. F_l can be disaggregated into a series of concentrated forces distributed along the spool surface. For a concentrated force applied at position a on a beam, the governing equation for the beam deflection is provided by Beléndez et al. (2002):

$$y = \frac{F(a,\theta) z^2}{6EI}(3a - z),\ (0 \le z \le a) \tag{14}$$

$$y = \frac{F(a,\theta) a^2}{6EI}(3z - a),\ (a \le z \le L) \tag{15}$$

where $F(a,\theta)$ denotes the concentrated force dependent on the position a and the angle θ. a represents the Z direction distance from the anchored end to the concentrated force, m. θ represents the angle formed with the Y direction, °.

For a cylindrical spool with identical bending stiffness in both the X and Y directions, if the beam experiences small deformations within its elastic range, the total deflection under multiple loads can be determined by superimposing the deflections caused by each individual load. The deflection at position under the combined action of fluid and contact forces is calculated as:

$$y = \int_0^a \int_0^{2\pi} \frac{F(z,\theta) z^2 (3a - z)}{6EI} \mathrm{d}\theta \mathrm{d}z + \int_a^L \int_0^{2\pi} \frac{F(z,\theta) a^2 (3z - a)}{6EI} \mathrm{d}\theta \mathrm{d}z \tag{16}$$

According to Han et al. (2017), the radial force F_l exerted by the fluid on the spool surface can be calculated by integrating the vertical component of the pressure as follows:

$$F_l = \int_0^L \int_0^{2\pi} p\cos(\alpha) d_1 \mathrm{d}\alpha \mathrm{d}z \tag{17}$$

where p represents the pressure experienced by the spool, MPa; and α represents the phase angle between pressure and F_l, °.

According to Han et al. (2017), the fluid force F_z can be expressed as:

$$F_z = F_s + F_d, \tag{18}$$

$$F_d = \int p_d S_c \tag{19}$$

where F_s is the static force, N; F_d is the dynamic force, N; p_d represents the dynamic pressure acting on the axial direction of the spool, MPa; and S_c denotes the axial projected area of the spool, m^2.

Fig. 7 illustrates the forces acting on the spool within the control valve. The spool is subjected to a combination of concentrated and distributed forces, which generate corresponding reactive forces at the support surface and within the valve body.

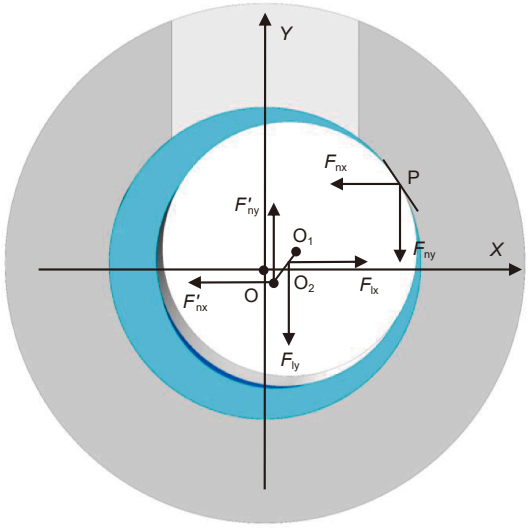

Fig. 7. The support force F'_n, contact force F_n and radial force F_l on the spool.

Accordingly, the force balance equation for the spool can be expressed as:

$$\begin{pmatrix} F'_{nx} \\ F'_{ny} \end{pmatrix} + \begin{pmatrix} F_{nx} \\ F_{ny} \end{pmatrix} + \begin{pmatrix} F_{lx} \\ F_{ly} \end{pmatrix} = \begin{pmatrix} 0 \\ 0 \end{pmatrix} \tag{20}$$

where F'_{nx} and F'_{ny} represent the X and Y components, respectively, of the support force F'_n acting on the support surface, N. Similarly, F_{nx} and F_{ny} denote the X and Y components of the F_n ,N, while F_{lx} and F_{ly} correspond to the X and Y components of F_l ,N.

The spool experiences friction because of F_n, which causes variations in F_z during movement. Thus, F_z experienced by the spool, caused by both fluid force and friction force F_f (N), is:

$$F = F_z \pm F_f \tag{21}$$

$$F_f = \mu F_n + \mu' F'_n \tag{22}$$

where μ is the friction coefficient of zirconia in water. F'_n represents the support force acting at transitional structure, μ' is the sliding friction coefficient of steel with lubricated contact.

Table 1 lists all the parameters required for the formulas.

5. Mechanical analysis numerical model

5.1. Meshing and boundary condition settings

The model dimensions and meshing methods were consistent with previous studies (Xu et al., 2024). Based on the COUPLED pressure-velocity coupling method and a fixed reference frame, a pressure correction equation was employed to iteratively update the pressure and velocity fields. The working flow was set as water, with a density of 998.2 kg/m^3 and a viscosity of 0.001 kg/(m·s). To simulate a typical pressure range, the inlet and outlet pressures were set at 20 and 15 MPa, respectively (Liu et al., 2017). Since the inlet pressure remained relatively stable and environmental interference is minimal, the turbulence intensity and turbulence viscosity ratio at both the inlet and outlet were set to 5% and 10%, respectively, to ensure a moderate level of turbulence. The wall surfaces were defined as no-slip walls. To replicate resistance in horizontal pipes, a standard roughness model was applied to the pipe walls. Given that the pipes were made of seamless hot-drawn steel, the roughness height and roughness constant were set to

Table 1
The parameter required for the energy consumption model.

Symbol	Description	Value
μ_b	Friction coefficient of the bearings	0.0015
F_b	Radial load on the bearing, N	100
d_b	Inner diameter of the bearing, mm	7
μ_s	Friction coefficient of the sealing system	0.05
h	Length of the sealing surface, mm	3.5
d_a	Diameter of the shaft, mm	7
p_s	Necessary sealing pressure, MPa	74
d_l	Mean diameter of the thread, mm	7.25
λ	Helix angle of the screw, °	3.78
ρ'	Equivalent friction angle, °	9.4
S	Lead, mm	1.5
P	Pitch, mm	1.5
γ	Number of threads	1
v	Axial movement velocity of the spool, mm/s	0.1
t	Stroke time, s	230
μ'	Sliding friction coefficient of steel with lubricated contact	0.19
μ	Friction coefficient of zirconia in water	0.35
E	Material's modulus of elasticity, GPa	193

0.07 and 0.5 mm , respectively (Xu et al., 2024). The fluid domain was simulated using the Realizable k-epsilon model, which is effective for flow prediction within narrow clearance regions (Han et al., 2017). Spatial discretization employed a second-order upwind scheme, and the residual convergence criterion was set at 1×10^{-5}, ensuring high accuracy in flow simulation.

For the solid domain, tetrahedral meshes were employed to automatically discretize the solid domain. The spool material was defined as zirconia ceramic, with material properties including a Young's modulus of 200 GPa and a Poisson's ratio of 0.3. The other components were modeled as seamless hot-drawn steel, with a Young's modulus of 193 GPa and a Poisson's ratio of 0.3. A rigid connection was established between the spool and the transition section, while fixed constraints were applied to the support surface to replicate real-world operational conditions. To simulate initial contact deformation, pre-displacement was applied to the valve body, generating an initial contact force on the spool. The spool surface was designated as the pressure input face, where the pressure results obtained from the fluid domain were applied to induce and analyze spool deformation.

5.2. Grid independence

The mechanical analysis model incorporates both fluid and solid domains, with the mesh resolution in each domain directly influencing the final simulation results. To ensure calculation accuracy, grid independence studies were conducted and verified. In the fluid domain, mesh density was specifically refined around the fit clearance region to ensure accurate pressure distribution on the spool surface. Similarly, in the solid domain, the grid density on the spool surface was increased to achieve precise displacement results. Fig. 8 shows the grid independence results. Increasing the grid number from 885,000 to 1,186,000 in the fluid domain, and from 942,000 to 1,217,000 in the solid domain showed that simulation outcomes remain consistent. Therefore, grid independence was achieved when the grid number exceeded 885,000 in the fluid domain and 942,000 in the solid domain, ensuring the robustness and reliability of the model predictions.

5.3. Validation

Building on our previous research, where a CFD model of the control valve was developed and validated against theoretical and experimental results (Xu et al., 2024), this study advances the modeling approach by treating the spool as an elastic body rather than a rigid one, with a particular focus on the implications of contact friction. The adoption of an elastic spool model aims to address previously overlooked phenomena, such as spool deformation and the influence of contact friction on valve performance.

To validate the numerical model, the control valve was modeled using the same size parameters as in the earlier study (Xu et al., 2024). The control valve's performance was primarily evaluated based on its flow coefficient C_v and surface pressure distribution. The comparison results, shown in Fig. 9, reveal deviations of −0.45% and −1.95% between the current simulation results and the experimental and theoretical data, respectively, with consistent pressure distribution profiles. Further validation was conducted through deformation analysis, specifically focusing on the Y-deformation at the spool end face, which serves as a critical indicator of the spool's elastic behavior under operational stresses. Theoretical results were obtained from Section 4.3. Fig. 10 shows that the deviation remains within 1.70%. These findings confirm the effectiveness of the developed model in accurately simulating flow characteristics and spool deformation behavior of the control valve.

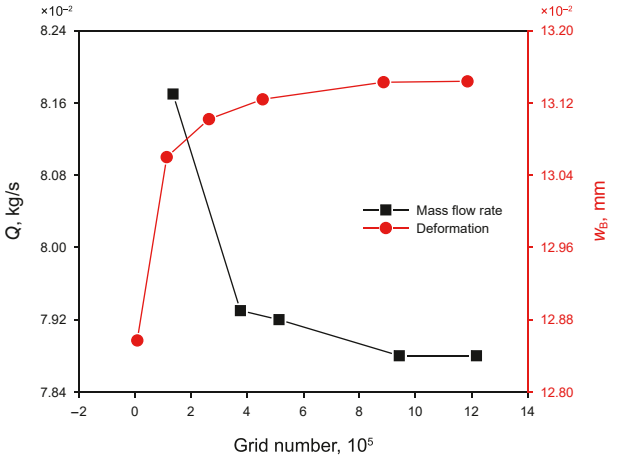

Fig. 8. Grid independence.

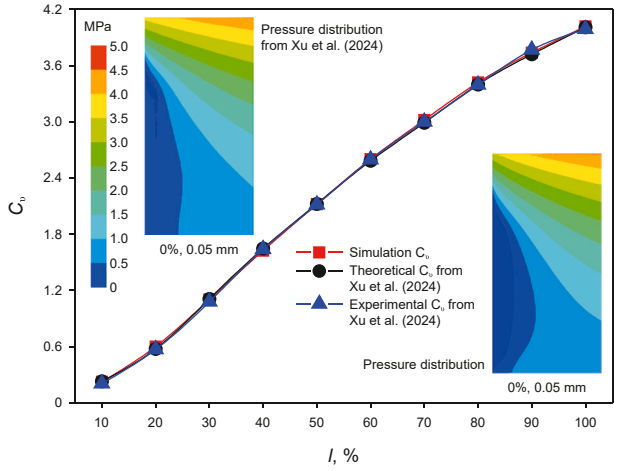

Fig. 9. The theoretical, experimental, and numerical results of flow coefficient C_v with different opening l.

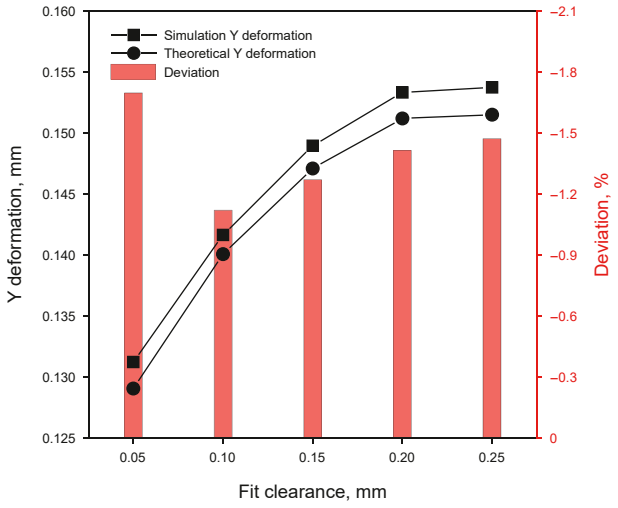

Fig. 10. Simulation and theory results of Y deformation and deviation with different fit clearance δ.

6. Results and discussion

The optimal design of fit clearance δ in control valves is crucial, requiring a balance between minimizing energy consumption and leakage. Our investigation identifies two critical states induced by spool posture: the extreme energy consumption state and the extreme leakage state. In the extreme energy consumption state, the spool tilts towards the outlet and undergoes significant deformation due to contact and fluid forces, resulting in maximized friction and energy consumption. Conversely, in the extreme leakage state, as the spool moves away from the outlet, flow resistance reaches a minimum, leading to maximum leakage.

These situations typically arise when the support surface of the transition section experiences maximum inclination within the *YZ* plane, causing contact deformation between the spool and the valve body. This behavior exemplifies complex FSI effects, influencing fluid distribution, force characteristics, and contact stress. Specifically, at $\alpha_1 = 0°$ and deflections of $e_1 = e_2 = 0.02$ mm, maximum energy consumption and friction forces were observed, whereas maximum leakage occurred at $\alpha_1 = 180°$ and $e_1 = e_2 = 0.02$ mm with the same deflections.

By isolating these critical parameters under extreme conditions, it becomes possible to ensure the long-term stable operation of control valves. The differentiated effects of spool posture on friction force, leakage, and energy consumption provide valuable insights for optimizing control valve designs to achieve enhanced performance and operational efficiency.

6.1. Case under the maximum friction force situation

6.1.1. Pressure contours

Fig. 11 shows the pressure contours for different deflection angles α_2 and fit clearance δ at $\alpha_1 = 0°$. The figure reveals that as δ decreases, the pressure distribution on the spool surface varies more significantly with α_2, resulting in the formation of a high-pressure zone. Based on prior boundary condition assumptions, under high pressure differentials, fluid flow is primarily pressure-driven, where inertial effects dominate, and viscous effects are negligible. This phenomenon can be explained using local pressure loss theory and Bernoulli's equation (Li et al., 2024).

Under a constant pressure differential, increasing δ enlarges the hydraulic diameter of flow passage, reduces the valve's flow resistance, and increases the flow velocity through the valve. According to Bernoulli's equation, velocity changes caused by local flow expansion reduce fluid kinetic energy losses, leading to a decrease in the pressure gradient. Consequently, this results in a reduction in radial force F_l acting on spools. The results indicate that the local maximum pressure on the spool reaches 19.75 MPa when $\delta = 0.05$ mm and $\alpha_2 \geq 135°$. At this point, the pressure difference across the spool surfaces is greatest, and according to Eq. (17), F_l reaches its maximum. This radial force F_l deforms the spool towards outlet, increasing contact friction with the valve body, thereby raising energy consumption. Therefore, increasing δ is beneficial for reducing energy consumption and promoting more stable fluid flow within clearance during optimization.

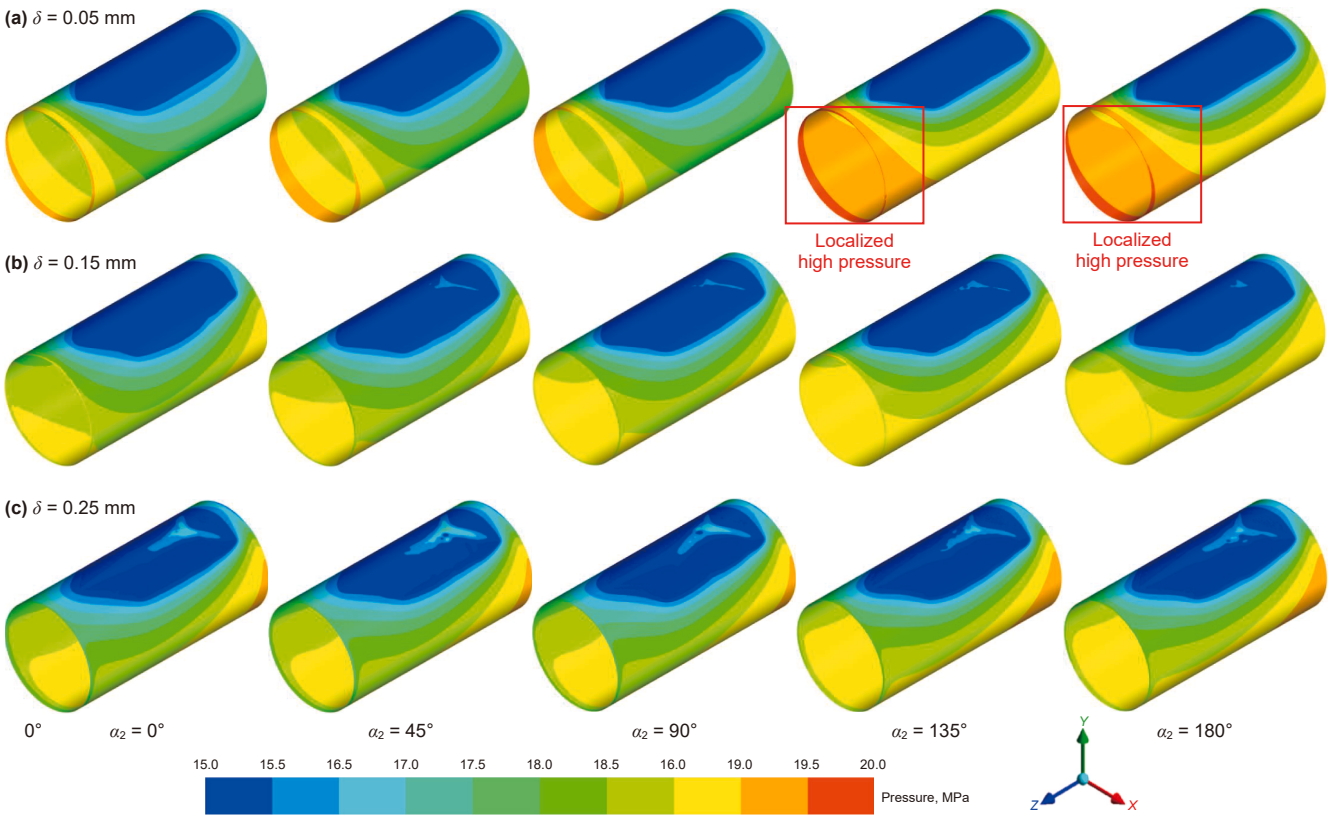

Fig. 11. Pressure contours with different deflection angle α_2, ranging from 0° to 180°, and various values of the fit clearance of (**a**) $\delta = 0.05$ mm, (**b**) $\delta = 0.15$ mm, and (**c**) $\delta = 0.25$ mm.

Jia and Su (2020) presented contour plots of the flow field on the spool surface under different fit clearances, ranging from 2 to 14 μm. Their comparison revealed that for small fit clearances, fluid flow is restricted, with friction and viscous effects dominating, resulting in relatively stable and smooth flow. Conversely, for larger fit clearances, fluid kinetic energy losses decrease, leading to higher flow velocities and increased fluid inertia effects. Xu et al. (2024) investigated gap flow of the spool under large fit clearances (ranging from 50 to 200 μm), but their study modeled the spool as a rigid body, neglecting the impact of solid deformation under high-pressure differentials. This assumption limits the ability to accurately capture the true fluid-structure interaction and restricts a detailed description of pressure distribution on the spool surface.

6.1.2. Force analysis of spool

Fig. 12 shows the friction force F_f, contact force F_n, support force F_n' for different deflection angles α_2 and fit clearance δ at $\alpha_1 = 0°$. The results indicate that as δ decreases, F_f increases significantly (up to 462.8 N) and varies markedly within α_2 range of 0°–180° (from 156.3 to 462.8 N). This behavior occurs because, with smaller δ, as α_1 increases, the spool's orientation relative to the valve body changes more drastically, resulting in significant increases in both F_n and F_n', as shown in Fig. 12(b) and (c). This interaction induces an elastic response along the radial direction of the spool, with the degree of deformation depending on the material's Young's modulus (Shi and Jar, 2022).

The bending deformation alters the spool's geometry, causing it to move closer to the lateral outlet, thereby increasing radial force F_l. This F_l further intensifies the elastic bending of the spool, leading to continued increases in F_n and F_n' until equilibrium is reached between F_l and F_n. According to Eq. (22), the increase in F_n leads to intensified F_f, resulting in greater frictional energy losses during spool movement. In contrast, increasing δ improves the contact interaction between the spool and valve body, reducing the spool's elastic deformation. This suppression of deformation helps stabilize F_f across varying α_2, thereby reducing overall energy consumption.

Compared to numerical models that only consider viscous friction (Nie et al., 2021), the model developed in this study more

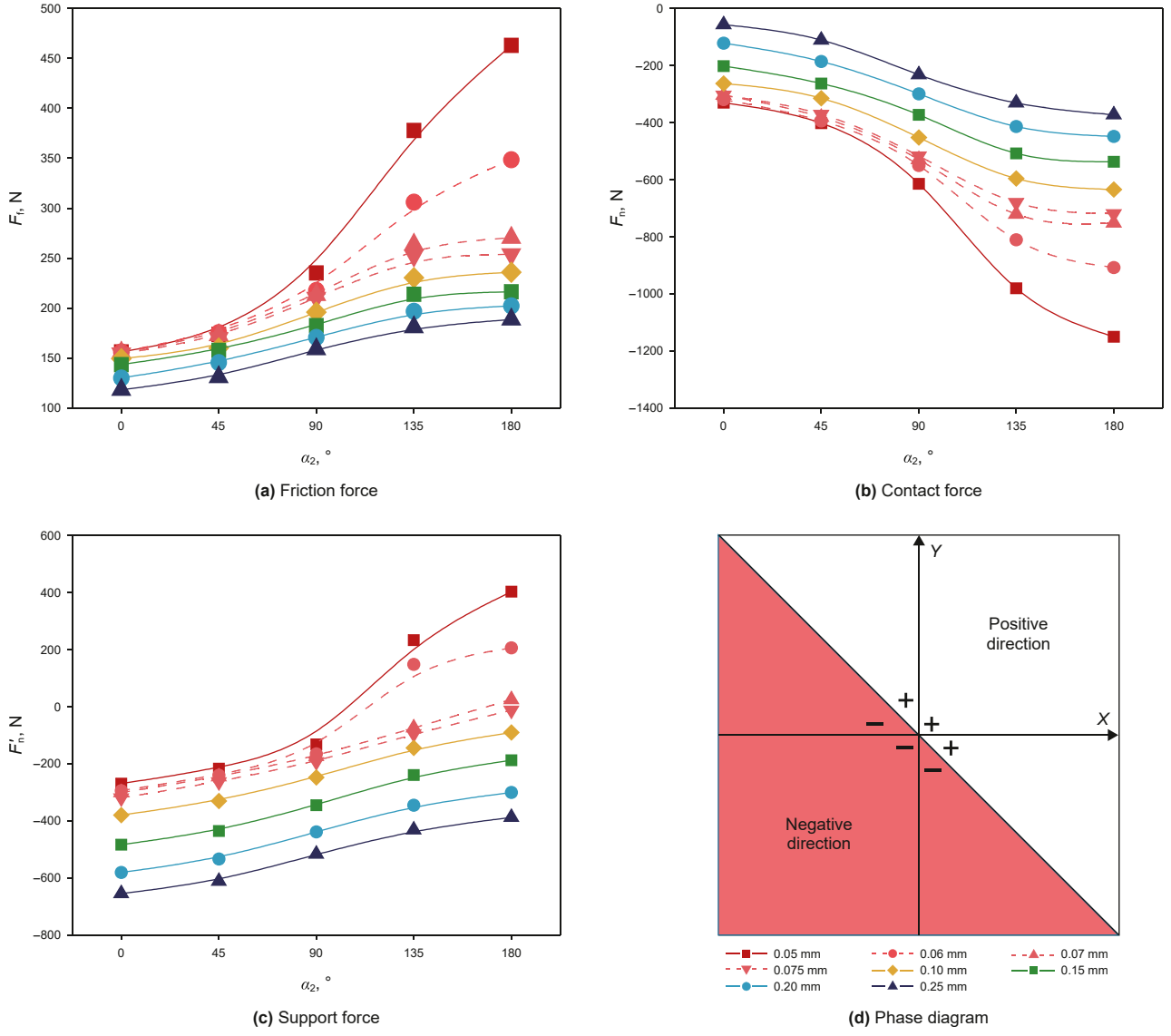

Fig. 12. Variation of (**a**) friction force F_f, (**b**) contact force F_n, and (**c**) support force F_n' with different deflection angle α_2 and fit clearance δ. The (**d**) refers to phase diagram.

accurately captures the force characteristics of the spool under solid-solid contact friction. Furthermore, the elastic deformation observed is caused by the coupling of initial contact forces and fluid forces, a phenomenon that cannot be accurately simulated by rigid spool models (Hong and Kim, 2016; Xu et al., 2024). Existing fluid-structure interaction simulations do not account for initial contact forces (Qian et al., 2014; Zhao et al., 2020, 2023). Thus, the model presented in this study provides a more realistic representation of the force and deformation mechanisms of the spool within the fit clearance, offering a precise numerical foundation for optimization design.

6.1.3. Equivalent stress

The equivalent stress provides insights into the scalar stress experienced during contact between the spool and the valve body, representing the stress level under complex stress conditions (Ludvigsen et al., 2021). In ANSYS, the equivalent stress is calculated using the von Mises stress criterion (Wang et al., 2021). Fig. 13 presents the equivalent stress distribution on the spool surface for different deflection angles α_2 and fit clearance δ at $\alpha_1 = 0°$. When $\delta < 0.075$ mm, as α_2 increases, the angular deviation of the spool relative to the valve body causes the contact area to expand from simple point contact to a larger surface area contact. This expansion results in localized compression and material squeezing at the surface material (contact surface 1 and contact surface 2), leading to localized stress concentration within the contact region.

These results indicate tighter contact between the spool and the valve body, which increases the contact force F_n. This not only affects the overall movement characteristics of the spool but also significantly increases the friction force F_f. Conversely, as δ increases, the contact area between the spool and the valve body

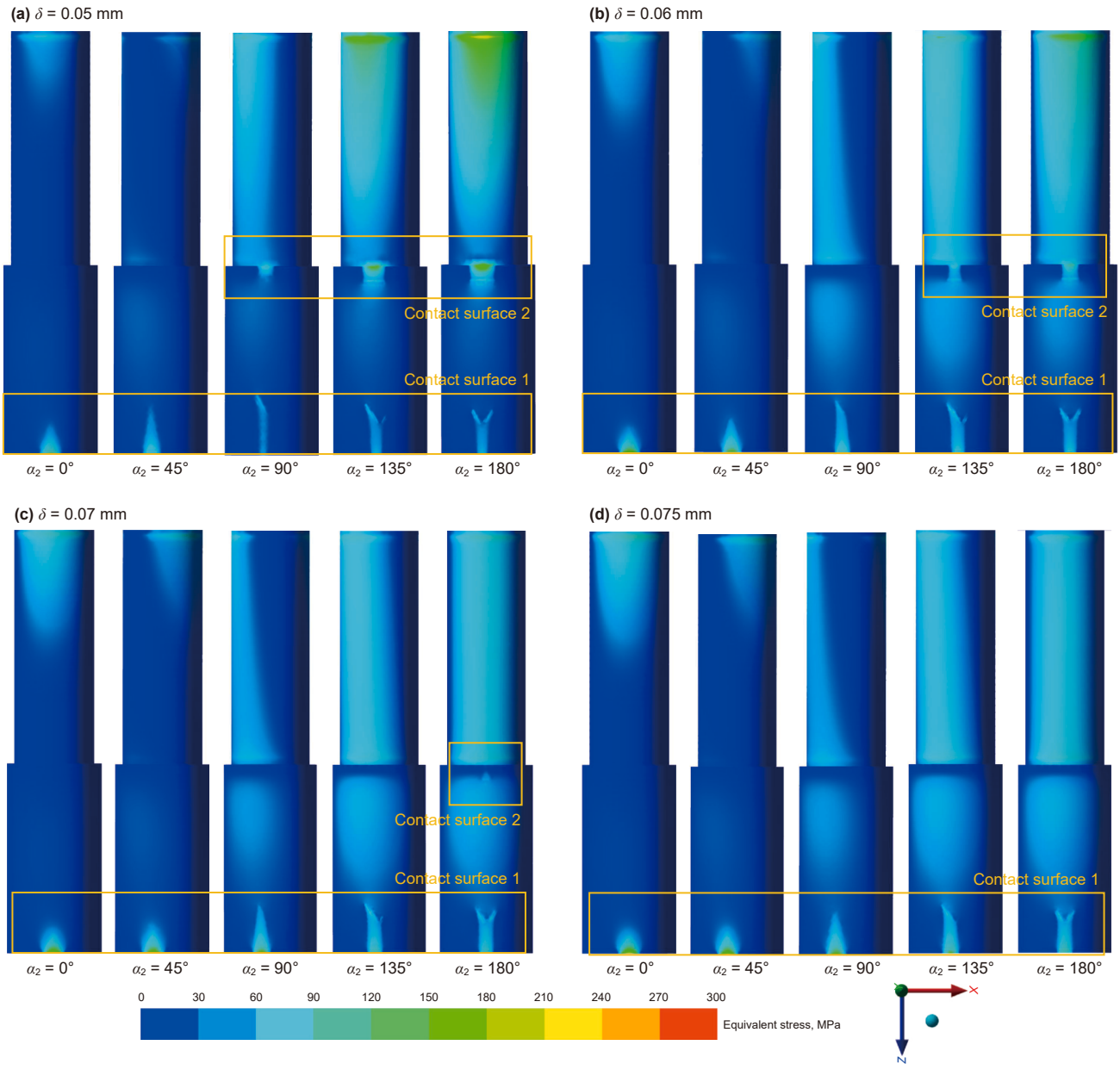

Fig. 13. Equivalent stress with different values of deflection angle α_2 and fit clearance of (**a**) $\delta = 0.05$ mm, (**b**) $\delta = 0.06$ mm, (**c**) $\delta = 0.07$ mm, (**d**) $\delta = 0.075$ mm.

decreases, resulting in a significant reduction in F_n. This weakens the solid-solid contact friction, thereby reducing the system's energy consumption.

6.2. Case under the maximum leakage situation

6.2.1. Pressure contours

Fig. 14 presents the pressure contours on the spool surface. When the $\delta = 0.05$ mm and $\alpha_2 \leq 90°$, a localized high-pressure region appears in the contact area between the spool and the lower wall of the valve body. This occurs due to the angular deflection of the spool relative to the valve body, which causes localized pressure concentration within the contact region. At this stage, fluid flow within the clearance is restricted, with potential energy reaching its maximum while kinetic energy decreases.

As δ increases, the fluid flow path within the clearance becomes smoother. A larger clearance reduces fluid's potential energy and increases its kinetic energy, thereby lowering the overall flow resistance. Consequently, the impact force of the fluid on the spool surface weakens, leading to an overall reduction in surface pressure and a more uniform pressure distribution.

From Figs. 11 and 14, it can be concluded that even slight deformation of the spool leads to significant changes in the pressure distribution within the clearance. This occurs because the bending deformation of the spool alters the fluid flow path and redistributes the local flow field within the clearance, causing the pressure gradient to shift. These changes in pressure distribution not only affect local force characteristics but also result in variations in the overall performance of the spool, particularly at different deflection angles.

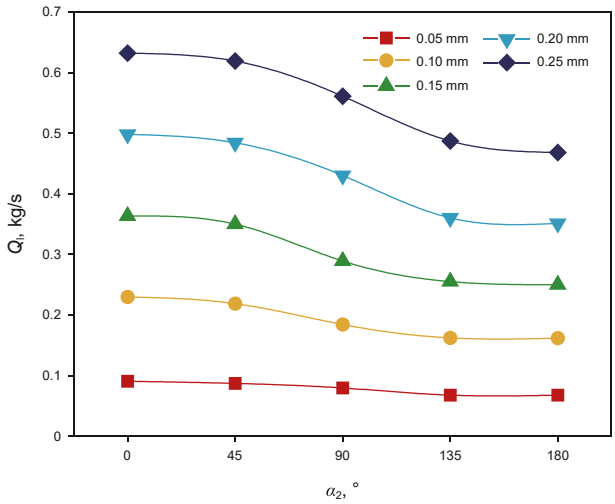

Fig. 15. Variation of leakage Q_l with different deflection angle α_2 and fit clearance δ.

6.2.2. Maximum leakage

Fig. 15 shows the leakage Q_l for different deflection angles α_2 and fit clearance δ at $\alpha_1 = 180°$. The results indicate that when α_2 increases from 0° to 180° and δ is small, Q_l is relatively high (up to 0.63 kg/s) and exhibits significant variation (ranging from 0.47 kg/s to 0.63 kg/s). According to the Darcy-Weisbach equation (Abdulameer et al., 2022), Q_l is inversely proportional to the flow resistance. Therefore, as α_2 increases, the spool gradually moves

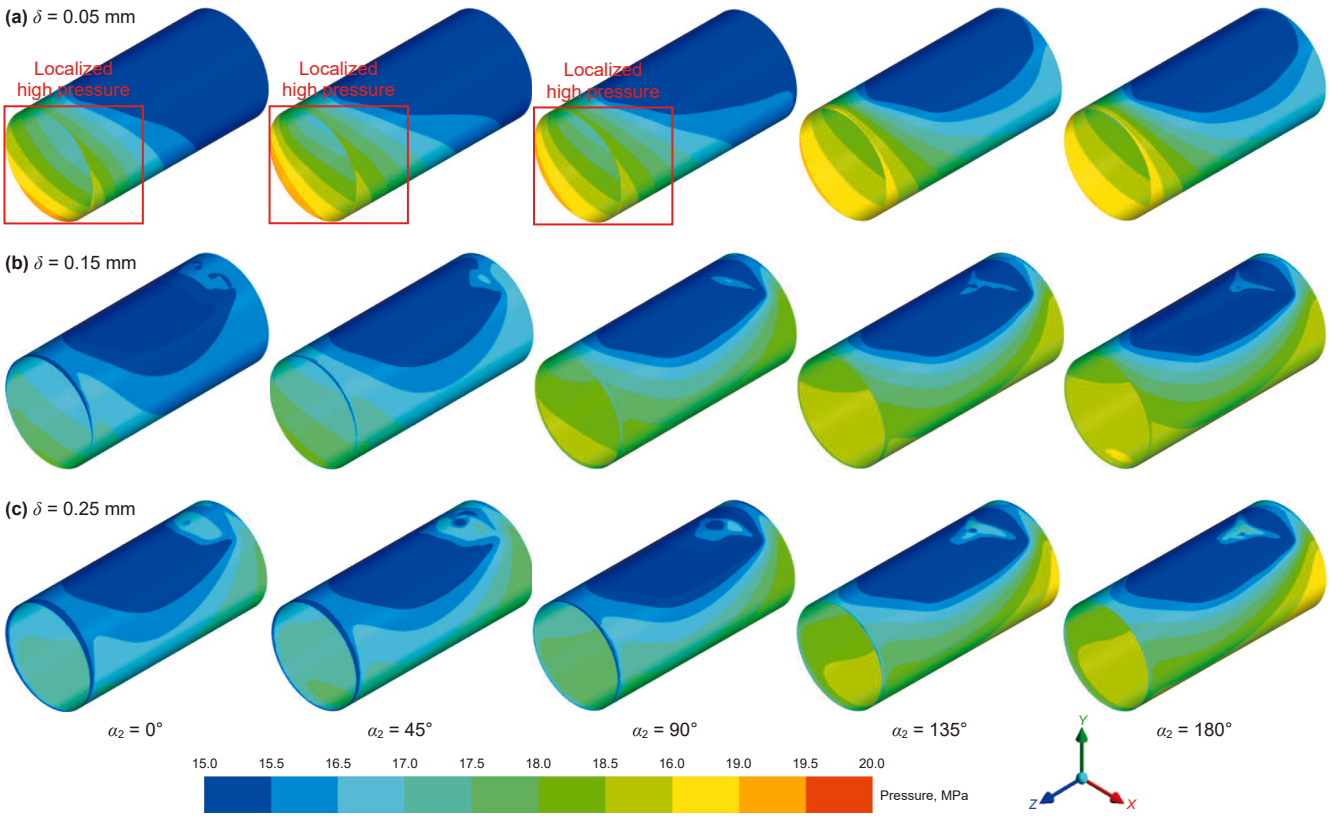

Fig. 14. Pressure contours with different values of phase angle α_2 and fit clearance of (**a**) $\delta = 0.05$ mm, (**b**) $\delta = 0.15$ mm, and (**c**) $\delta = 0.25$ mm.

closer to the outlet, reducing the hydraulic diameter, which increases flow resistance and lowers Q_l.

When δ is larger, the hydraulic diameter increases, leading to an overall reduction in valve flow resistance. The relative impact of α_2 on flow resistance also becomes more pronounced, resulting in greater variation in Q_l. Additionally, because of the inherent randomness and uncertainty in the spool's deflection (i.e., α_2 value) under practical conditions, Q_l becomes extremely sensitive to slight misalignments, causing significant fluctuations in flow rate. These random flow variations not only complicate flow control but also introduce additional energy losses.

Moreover, a larger Q_l corresponds to a lower flow regulation rate, making it difficult for the valve to maintain the desired flow output accurately. Specifically, when δ is 0.25 mm, the flow regulation rate is 90.81%, leaving 9.09% of the flow range unregulated. In contrast, a 0.05 mm clearance achieves a regulation rate of 98.68%.

Therefore, to maintain a stable Q_l under varying α_2, δ should be appropriately reduced to minimize fluctuations in the hydraulic diameter and associated changes in flow resistance. Currently, the applicability of leakage formulas for annular gaps is mostly limited to regular annular clearances (Zhao et al., 2020). For example, Zhao et al. (2023) theoretically derived the leakage rate considering eccentricity and structural deformation within fit clearance. However, due to the presence of a lateral outlet in this study, theoretical modeling becomes challenging, while numerical models offer a simpler and more accurate approach. Most existing studies overlook the impact of contact deformation on valve flow resistance, potentially biasing Q_l results (Li and Wu, 2020; Zhao et al., 2023). By accounting for spool contact deformation, the

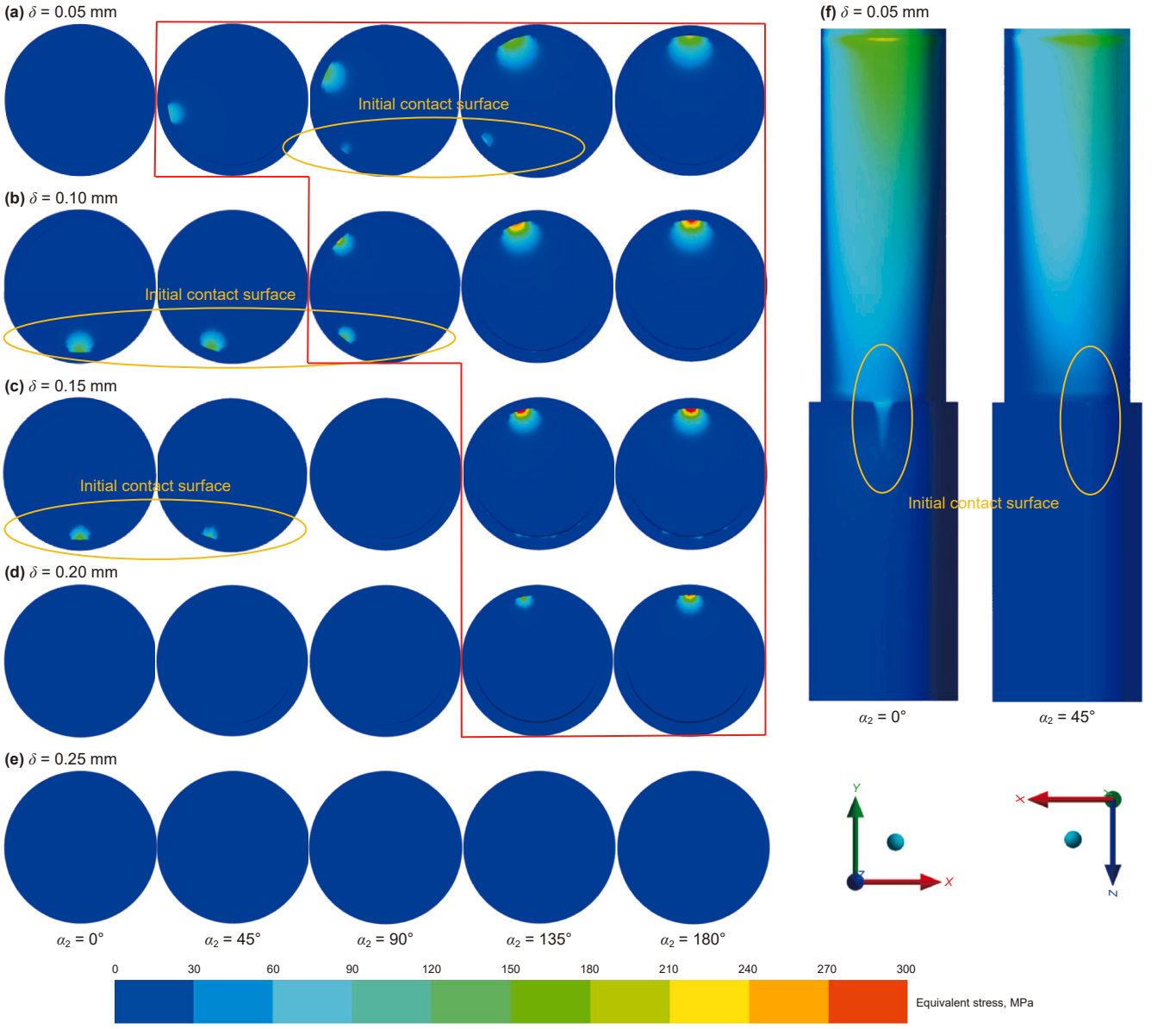

Fig. 16. Equivalent stress with different deflection angle α_2 and fit clearance of (**a**) $\delta = 0.05$ mm, (**b**) $\delta = 0.10$ mm, (**c**) $\delta = 0.15$ mm, (**d**) $\delta = 0.20$ mm, (**e**) $\delta = 0.25$ mm, (**f**) $\delta = 0.05$ mm. Diagrams within yellow frames show the contact surface's position under contact force F_n. Specifically, when $\delta = 0.05$ mm and α_2 are respectively 0° and 45°, the positions are as shown in Fig. 16(f). Conversely, diagrams outside yellow frames represent cases where the spool has no contact surfaces. Diagrams within the red frames represents final contact positions under combined effects of fluid force and contact force F_n. Conversely, diagrams outside red frames represent that the spool has no contact surfaces.

model developed in this study provides more accurate Q_l predictions, offering crucial guidance for optimizing leakage performance in control valve design.

6.2.3. Equivalent stress

Fig. 16 shows the equivalent stress distribution of the spool under different α_2 and fit clearance δ at $\alpha_1 = 180°$. When δ is small, the contact between the spool and valve body becomes tighter. In this case, the contact force F_n primarily acts on the initial contact area of the spool (highlighted in the yellow frames in Fig. 16), leading to localized stress concentration. As fluid forces act on the spool, they cause the spool to tilt and shift in the direction of the applied force. The radial force F_l exerted by the fluid is relatively large, driving the spool to tilt toward the outlet. This tilting causes the contact area to shift from the lower left to the upper left (as indicated by the red frames in Fig. 16), forming a new region of stress concentration.

The localized stress concentration induces bending deformation of the spool and alters the geometry of the contact surface. When δ is larger, the gap between the spool and the valve body increases, significantly reducing the contact area. The regions outside the red frames in Fig. 16 illustrate that under these conditions, no distinct contact surface forms between the spool and valve body. This behavior occurs because a larger δ provides the spool with greater freedom of movement within the valve body, thereby reducing the effects of localized stress concentration.

6.2.4. Force analysis of spool

Fig. 17 shows contact force F_n and support force F'_n for different deflection angles α_2 and fit clearance δ at $\alpha_1 = 180°$. Fig. 17(a) shows that when δ is small, F_n gradually decreases as the α_2 increases, reaching its lowest point at $\alpha_2 = 180°$. This indicates that as the spool deflects and tilts toward the outlet, the contact forces on the spool redistribute. For larger δ, F_n remains more consistent, exhibiting less variation as α_2 changes. This suggests that with a larger δ, the spool's contact with the valve body becomes more flexible, increasing its degrees of freedom, making F_n less sensitive to α_2 variations, thereby reduces stress concentration.

Fig. 17(b) shows that with a small δ, F'_n decreases significantly as α_2 increases. This behavior suggests that as α_2 increases, the opposing actions of F_l and F_n prevent F'_n from varying as drastically compared to conditions with a larger δ. As δ increases, the downward trend of F'_n becomes more pronounced. This occurs because a larger δ enhances the spool's freedom of movement, allowing F_l to be fully balanced by F'_n.

Fig. 17 also indicates that F_n, induced by spool deflection, and radial force F_l act in opposite directions, resulting in a lower net force on the spool compared to the conditions observed in Fig. 12. This suggests a potential optimization strategy: precisely controlling α_2 could help minimize friction and energy consumption. However, even minor changes in α_2 result in significant variations in force distribution. Nonetheless, achieving extremely high precision in α_2 may not be feasible in large-scale manufacturing. This analysis highlights the primary optimization direction of this study: improving energy efficiency through appropriate δ design adjustments rather than relying on extremely tight machining tolerances.

6.3. Case under the energy consumption situation

Fig. 18 shows variation of friction force F_f and axial force F_l for different opening l and fit clearance, evaluated under the conditions of maximum F_f at $\alpha_1 = 0°$ and $\alpha_2 = 180°$. Fig. 18 reveals that the opening range of [0%, 30%] represents a danger zone, where the spool experiences maximum F_f, along with greater radial and contact forces (as shown in Fig. 12(b) and (c)] and stress concentration in the contact region (as shown in Fig. 13). These combined effects could potentially lead to sticking and operational difficulties (Yu et al., 2024). Since existing control valves often operate at low openings (Zhang et al., 2022), increasing δ can mitigate the high friction phenomenon in low-opening range, thereby reducing the likelihood of sticking and lowering maintenance costs.

As shown in Fig. 18(b), axial force F_z gradually decreases as the valve opening l increases, indicating a reduced impact of the fluid on spool's end face. However, as l further increases, fluid accumulation on the lower end face of spool expands, generating a localized high-pressure region, causing a slight increase in F_z.

The maximum single-stroke energy consumption and full-stroke energy consumption U of the control valve for different fit clearance δ were calculated using Eqs. (11)–(18), as shown in Fig. 19. Fig. 19 shows that during the forward stroke, the maximum single-stroke U with a δ of 0.05 mm is 9.25% higher than with a 0.25 mm clearance, while during the return stroke, it is 2.86% lower. The maximum full stroke U with a 0.05 mm clearance

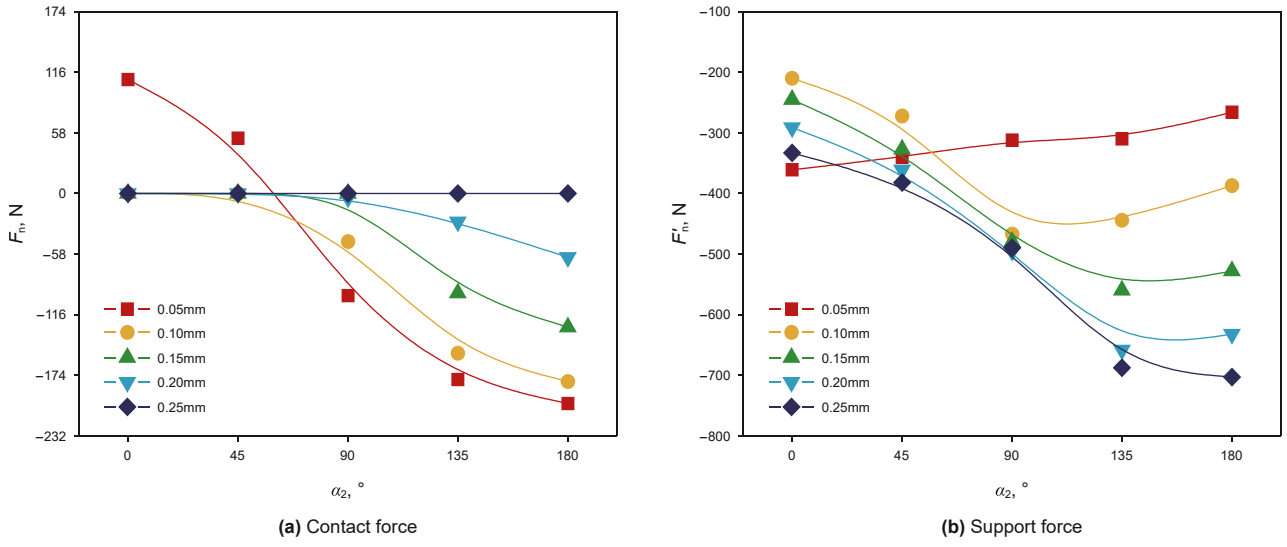

Fig. 17. Variation of (**a**) contact force F_n, (**b**) support force F'_n with different deflection angle α_2 and fit clearance δ.

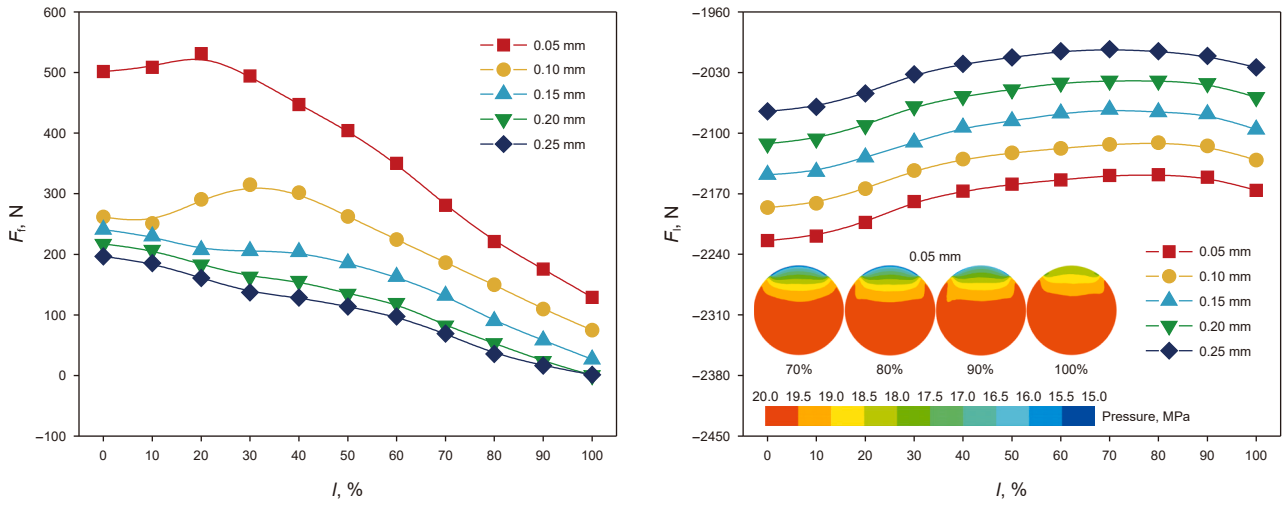

(a) Friction force **(b)** Axial force

Fig. 18. Variation of (**a**) friction force F_f and (**b**) axial force F_l with different opening l and fit clearance δ.

is 3.33% higher than that with a 0.25 mm clearance. For independent driving U (excluding contributions from sealing, bearings, and motion conversion), the three key results are 19.58%, 6.89%, and 7.21%, respectively.

The results indicate that δ has a greater influence on the independent driving energy consumption U, primarily due to the dilution effect of sealing energy consumption, which accounts for at least 46.25% of the total full stroke U. Sealing energy consumption is mainly influenced by the fluid pressure differentials, the friction coefficient of the sealing material, and the flow resistance through the seal. Valves operating under higher pressure conditions require stronger sealing to prevent leakage, which in turn increases friction at the sealing surface. In contrast, under lower pressure conditions, sealing energy consumption is reduced, making the optimization of δ more effective in decreasing frictional losses and improving energy efficiency.

6.4. Optimization design

Due to randomness of deflection and deformation, optimizing fit clearance is an effective strategy for reducing energy consumption. A small fit clearance not only expands the high-pressure zone and increases radial force but also induces significant spool deformation, leading to elevated friction and higher energy consumption. Conversely, a larger fit clearance can cause substantial leakage, with notable variations across different deflection angles. Total energy consumption exhibits a roughly linear relationship with fit clearance, which fails to adequately capture frictional characteristics (as shown in Fig. 19). In contrast, the friction force curve more accurately reflects the features of energy consumption (as seen in Fig. 18(a)) and is closely linked to valve reliability. Therefore, a trade-off between minimizing friction force and leakage is employed to determine the optimal fit clearance, aiming to achieve the lowest overall energy consumption.

In this study, a genetic algorithm is utilized to optimize the fit clearance δ (Alhijawi and Awajan, 2024). Based on data from Figs. 15 and 18(a), a cubic fitting function for maximum leakage and maximum friction force relative to δ is established and normalized, with raw data converted into dimensionless values. Objective variables are assigned equal weights, and the constraint range for the design parameter δ is set to [0.05 mm, 0.25 mm]. The fitness function is obtained by summing the normalized fitting functions of maximum leakage and friction force. A uniform distribution initialization is used to generate an initial population,

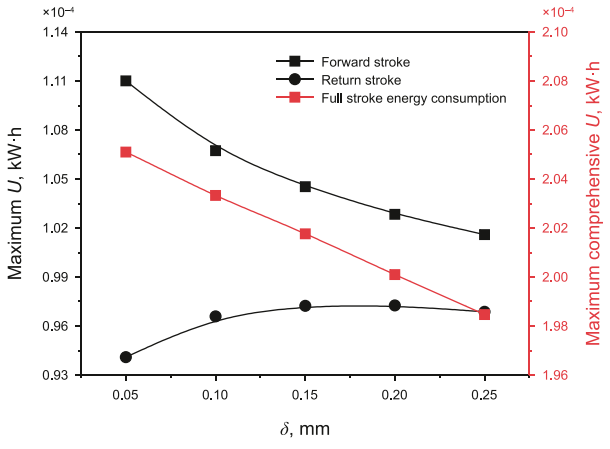

Fig. 19. Variation of maximum single-stroke energy consumption and total energy consumption U with different fit clearance δ.

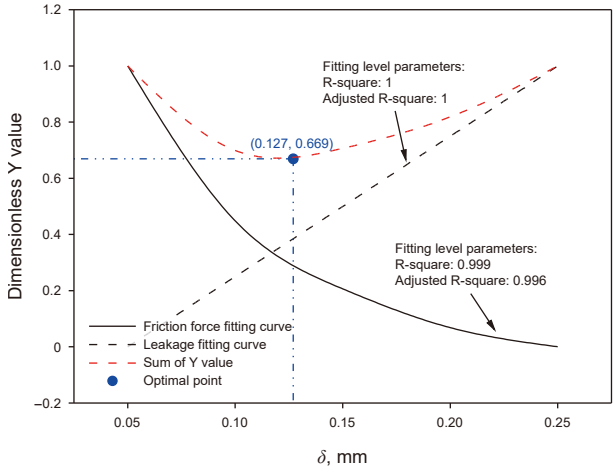

Fig. 20. Fitting curve and optimization results.

ensuring population diversity (Lipowski and Lipowska, 2012). The fitness of each individual is then evaluated according to the fitness function, and a proportion of individuals is selected for crossover and mutation. If the minimum value of fitness function is obtained, the optimal solution is returned; otherwise, newly generated individuals are added to the population, and the process is re-evaluated. Specific parameter settings are: Initial population:100; Generations: 200; Crossover rate: 0.8; Mutation rate: 0.2; Stopping conditions: maximum generation or optimal value.

Fig. 20 displays the fitting curves and optimal fit clearance results. Fig. 20 shows that the minimum value of the fitness function is 0.669, and corresponding optimal fit clearance is 0.127 mm. This fit-clearance value is selected by balancing the trade-off between minimizing friction force and leakage. It prevents the formation of a high-pressure zone at the bottom of the spool, thereby maintaining low radial forces (as shown in Fig. 11). It also avoids significant variations in frictional forces during spool deflection, keeping friction levels low (as shown in Fig. 12), thus suppressing high energy consumption. Under this clearance, the spool avoids forming multiple contact surfaces with the valve body (as seen in Fig. 13).

Although the leakage requirements for water injection applications are relatively low, this optimization effectively minimizes leakage and suppresses leakage fluctuations caused by spool deflection (as shown in Fig. 15). In summary, this optimal clearance not only prevents the valve from operating under extreme conditions but also improves energy efficiency.

7. Conclusions

Current fit clearance designs do not comprehensively consider both energy consumption and reliability, which limits the operational lifespan of wireless intelligent water distributors. Our study addresses this challenge by presenting a comprehensive analysis and employing a full-stroke energy consumption model to optimize design of fit clearance. The key findings are summarized as follows:

(1) The loosely coupled fluid-structure interaction (FSI) algorithm enables alternating analyses of fluid and solid domains while preserving their relative independence. This approach can effectively capture contact friction and spool deformation, allowing for detailed mechanical analysis and accurate assessments of leakage and energy consumption. The approach not only reduces computational time and simplifies the FSI interaction process but also offers high precision and practical value for future spool design and performance improvements.

(2) When the fit clearance is small, the spool deflects toward the outlet, causing significant unevenness in surface pressure distribution and generating substantial radial forces. At this point, contact between the spool and valve body leads to localized stress concentration, requiring higher energy consumption to drive the spool. Conversely, when the spool deforms away from the outlet, the pressure distribution becomes more uniform, reducing the total force on the spool and thus lowering energy consumption. However, with a larger fit clearance, the valve exhibits higher leakage rates and greater sensitivity to deflection angle variations.

(3) Under small clearance conditions, friction forces caused by random deflection and spool deformation are significant, leading to increased energy consumption. For instance, total energy consumption for one full stroke with a 0.05 mm clearance is 3.33% higher than with a 0.25 mm clearance. When the spool is independently driven, this difference increases to 7.21%. These results indicate that optimizing fit clearance is critical for enhancing energy efficiency, particularly in valves operating at low nominal pressure.

(4) The optimized fit clearance of 0.127 mm effectively prevents multiple surface contacts between the spool and valve body, maintaining low friction levels and stability. This optimization also suppresses the formation of high-pressure regions and danger zones associated with high friction, minimizes leakage, and enhances operational reliability. These improvements provide valuable design guidance for wireless intelligent water distributors and offer broader applicability to wired intelligent water distribution systems.

The findings and models developed in this study provide a robust theoretical framework and practical strategies for optimizing control valve fit clearance design. By balancing energy consumption and mechanical reliability, the optimized fit clearance enhances the overall performance and extends the service life of intelligent water distribution systems. These advancements have significant implications for reducing energy consumption, improving operational efficiency, and promoting sustainable development in intelligent oilfields operations.

For future research, the application of machine learning-based optimization algorithms could be explored to efficiently determine optimal fit clearance parameters tailored to various operating conditions. Additionally, larger-scale experimental validations should be conducted to further verify the robustness of the model and expand its application to other intelligent fluid control systems.

CRediT authorship contribution statement

Ning Xu: Methodology, Software, Validation, Formal analysis, Writing – original draft, Investigation. **Shi-Min Zhang:** Funding acquisition, Supervision. **De-Li Jia:** Resources. **Kun Tian:** Resources. **Yan-Hong Wei:** Resources. **Xiao-Xiao Zhu:** Methodology, Software. **Peichun Amy Tsai:** Writing – review & editing, Methodology, Resources, Software, Supervision.

Declaration of competing interest

The authors declare that they have no known competing financial interests or personal relationships that could have appeared to influence the work reported in this paper.

Acknowledgement

This work was supported by China Scholarship Council (CSC) (No. 202306440123).

Data availability

Data will be made available on request.

References

Abdulameer, L.S., Dzhumagulova, N., Algretawee, H., Zhuravleva, L., Alshammari, M.H., 2022. Comparison between Hazen-Williams and Darcy-Weisbach equations to calculate head loss through conveyancing treated wastewater in Kerbala city, Iraq. East.-Eur. J. Enterp. Tech 1 (1), 115. https://doi.org/10.15587/1729-4061.2022.251385.

Alhijawi, B., Awajan, A., 2024. Genetic algorithms: Theory, genetic operators, solutions, and applications. Evol. Intell. 17 (3), 1245–1256. https://doi.org/10.1007/s12065-023-00822-6.

Amirante, R., Catalano, L.A., Poloni, C., Tamburrano, P., 2014. Fluid-dynamic design optimization of hydraulic proportional directional valves. Eng. Optim. 46 (10), 1295–1314. https://doi.org/10.1080/0305215X.2013.836638.

Asim, T., Oliveira, A., Charlton, M., Mishra, R., 2019. Improved design of a multi-stage continuous-resistance trim for minimum energy loss in control valves. Energy 174, 954–971. https://doi.org/10.1016/j.energy.2019.03.041.
Beléndez, T., Neipp, C., Beléndez, A., 2002. Large and small deflections of a cantilever beam. Eur. J. Phys. 23 (3), 371. https://doi.org/10.1088/0143-0807/23/3/317.
Bucelli, M., Gabriel, M., Quarteroni, A., Gigante, G., Vergara, C., 2023. A stable loosely-coupled scheme for cardiac electro-fluid-structure interaction. J. Comput. Phys. 490, 112326. https://doi.org/10.1016/j.jcp.2023.112326.
Chen, L., Zhang, C., Jin, B., Yuan, T.B., 2023a. Simulation and experimental research on steady flow force compensation for a servo proportional valve. Flow Meas. Instrum. 94, 102457. https://doi.org/10.1016/j.flowmeasinst.2023.102457.
Chen, X.F., Yan, L., Gao, X.S., 2023b. Analysis and design of the optimal radius gap of the piston pair. Phys. Fluids 35 (11). https://doi.org/10.1063/5.0166098.
Ding, X.K., Wang, L.T., Cai, J.R., Wang, Z.H., Zhang, Z.X., Fan, X.Y., 2024. The sealing performance and failure analysis of marine valve packing seal structures based on dimensionless function definition. Ocean. Eng. 316, 119939. https://doi.org/10.1016/j.oceaneng.2024.119939.
Farhat, C., Van der Zee, K.G., Geuzaine, P., 2006. Provably second-order time-accurate loosely-coupled solution algorithms for transient nonlinear computational aeroelasticity. Comput. Methods Appl. Mech. Eng. 195 (17–18), 1973–2001. https://doi.org/10.1016/j.cma.2004.11.031.
Gigante, G., Vergara, C., 2021. On the stability of a loosely-coupled scheme based on a Robin interface condition for fluid-structure interaction. Comput. Math. Appl. 96, 109–119. https://doi.org/10.1016/j.camwa.2021.05.012.
Guo, S.L., Feng, Y.L., Tao, W.Q., 2017. Deviation analysis of loosely coupled quasi-static method for fluid-thermal interaction in hypersonic flows. Comput. Fluids 149, 194–204. https://doi.org/10.1016/j.compfluid.2017.03.017.
Han, M.X., Liu, Y.S., Wu, D.F., Zhao, X.F., Tan, H.J., 2017. A numerical investigation in characteristics of flow force under cavitation state inside the water hydraulic poppet valves. Int. J. Heat Mass Transf. 111, 1–16. https://doi.org/10.1016/j.ijheatmasstransfer.2017.03.100.
Hong, S.H., Kim, K.W., 2016. A new type groove for hydraulic spool valve. Tribol. Int. 103, 629–640. https://doi.org/10.1016/j.triboint.2016.07.009.
Jia, Y.S., Su, D.H., 2020. Analysis of clearance flow field of integrated mechanical-hydraulic servo spool valve for fan. J. Mech. Electr. Eng. 37 (9), 1099–1103. https://doi.org/10.3969/j.issn.1001-4551.2020.09.019 (in Chinese).
Kang, J.X., Lu, Y.J., Yang, X.L., Zhao, X.W., Zhang, Y.F., Xing, Z.G., 2022. Modeling and experimental investigation of wear and roughness for honed cylinder liner during running-in process. Tribol. Int. 171, 107531. https://doi.org/10.1016/j.triboint.2022.107531.
Kong, X.W., Wang, X.C., Ruan, X.F., Ren, Y.M., 2018. Optimum design of fit clearance of proportional cartridge valve. Adv. Mech. Eng. 10 (3). https://doi.org/10.1177/1687814018768168, 1687814018768168.
Kudela, J., Matousek, R., 2022. Recent advances and applications of surrogate models for finite element method computations: A review. Soft Comput. 26 (24), 13709–13733. https://doi.org/10.1007/s00500-022-07362-8.
Lei, Q., Weng, D.W., Luo, J.H., Zhang, J.J., Li, Y.L., Wang, X., Guan, B.S., 2019. Achievements and future work of oil and gas production engineering of CNPC. Petrol. Explor. Dev. 46 (1), 145–152. https://doi.org/10.1016/S1876-3804(19)30014-X.
Li, H.Y., Lu, H.N., Li, Q.S., 2024. Numerical investigations of the influences of valve spool structure on the eccentric jet flow characteristic in high-pressure angle valves. Energy 298, 131378. https://doi.org/10.1016/j.energy.2024.131378.
Li, L., Wu, J.B., 2020. Deformation and leakage mechanisms at hydraulic clearance fit in deep-sea extreme environment. Phys. Fluids 32 (6), 067115. https://doi.org/10.1063/5.0009913.
Lipowski, A., Lipowska, D., 2012. Roulette-wheel selection via stochastic acceptance. Physica A 391 (6), 2193–2196. https://doi.org/10.1016/j.physa.2011.12.004.
Liu, H., Pei, X.H., Jia, D.L., Sun, F.C., Guo, T., 2017. Connotation, application and prospect of the fourth-generation separated layer water injection technology. Petrol. Explor. Dev. 44 (4), 644–651. https://doi.org/10.1016/S1876-3804(17)30073-3.
Liu, H., Zheng, L.C., Yu, J.Q., Ming, E.Y., Yang, Q.H., Jia, D.L., Cao, G., 2023. Development and prospect of downhole monitoring and data transmission technology for separated zone water injection. Petrol. Explor. Dev. 50 (1), 191–201. https://doi.org/10.1016/S1876-3804(22)60380-X.
Liu, Q.T., Yin, F.L., Nie, S.L., Hong, R.D., Ji, H., 2021. Multi-objective optimization of high-speed on-off valve based on surrogate model for water hydraulic manipulators. Fusion Eng. Des. 173, 112949. https://doi.org/10.1016/j.fusengdes.2021.112949.
Liu, Y.S., Ren, X.J., Wu, D.F., Li, D.L., Li, X.H., 2016. Simulation and analysis of a seawater hydraulic relief valve in deep-sea environment. Ocean. Eng. 125, 182–190. https://doi.org/10.1016/j.oceaneng.2016.06.032.
Ludvigsen, S., Andleeb, Z., Khawaja, H.A., Moatamedi, M., Alzahabi, B., 2021. Multiphysics analysis of contact pressure profile of airless tires as compared to conventional tires. In: Multiphysics Simulations in Automotive and Aerospace Applications. Academic Press. https://doi.org/10.1016/B978-0-12-817899-7.00006-X.
Luo, Y.X., Lin, Z.H., Mu, J., Qian, J.Y., 2022. Research progress of spool stuck. Mech. Electr. Eng. 39 (7), 866–876. https://doi.org/10.3969/j.issn.1001-4551.2022.07.001 (in Chinese).
Ming, E., Yu, J.Q., Zheng, L.C., Lan, H.Q., Zhou, Q.C., Pei, X.H., 2023. Transmission model of transient flow wave signal in intelligent layered water injection system. J. Pet. Explor. Prod. Technol. 13 (9), 1935–1950. https://doi.org/10.1007/s13202-023-01658-7.
Nie, S.L., Guo, M., Yin, F.L., Ji, H., Ma, Z.H., Hu, Z., Zhou, X., 2021. Research on fluid-structure interaction for piston/cylinder tribopair of seawater hydraulic axial piston pump in deep-sea environment. Ocean. Eng. 219, 108222. https://doi.org/10.1016/j.oceaneng.2020.108222.
Qian, D., Liao, R.D., 2014. A nonisothermal fluid-structure interaction analysis on the piston/cylinder interface leakage of high-pressure fuel pump. J. Tribol. 136 (2), 021704. https://doi.org/10.1115/1.4026501.
Qian, J.Y., Xu, J.X., Zhong, F.P., Lin, Z.H., Hua, T.F., Jin, Z.J., 2023. Solid-liquid flow characteristics and sticking-force analysis of valve-core fitting clearance. J. Zhejiang Univ. – Sci. A. 24 (12), 1096–1105. https://doi.org/10.1631/jzus.A2300061.
Rao, A., 2003. Fluid-Solid Interaction Analysis Using ANSYS/Multiphysics. Elsevier Science Ltd. https://doi.org/10.1016/B978-008044046-0.50364-X.
Shi, F.R., Jar, P.B., 2022. Characterization of polyethylene using a new test method based on stress response to relaxation and recovery. Polymers 14 (14), 2763. https://doi.org/10.3390/polym14142763.
Simic, M., Herakovic, N., 2015. Reduction of the flow forces in a small hydraulic seat valve as alternative approach to improve the valve characteristics. Energy Convers. Manag. 89, 708–718. https://doi.org/10.1016/j.enconman.2014.10.037.
Souli, M., Ouahsine, A., Lewin, L., 2000. ALE formulation for fluid-structure interaction problems. Comput. Methods Appl. Mech. Eng. 190 (5–7), 659–675. https://doi.org/10.1016/S0045-7825(99)00432-6.
Wang, H.H., Lin, N.M., Yuan, S., Liu, Z.Q., Yu, Y., Zeng, Q.F., Fan, J.F., Li, D.Y., Wu, Y.C., 2024. Structural improvement, material selection and surface treatment for improved tribological performance of friction pairs in axial piston pumps: A review. Tribol. Int., 109838 https://doi.org/10.1016/j.triboint.2024.109838.
Wang, Q.B., Jia, D.L., Hu, G.X., Sun, F.C., Zhang, J.Q., 2020. Pressure wave downhole communication technique for smart zonal water injection. SPE Asia Pacific Oil and Gas Conference and Exhibition, Australia. https://doi.org/10.2118/202349-MS.
Wang, Y.Z., Li, G.Q., Wang, Y.B., Lyu, Y.F., 2021. Simplified method to identify full von Mises stress-strain curve of structural metals. J. Constr. Steel Res. 181, 106624. https://doi.org/10.1016/j.jcsr.2021.106624.
Wu, Y.N., Li, J.Y., Li, X.F., Huang, Y.X., Li, Y.Y., Cheng, L., 2024. Simulation analysis of flow characteristics of improved rectangular throttling groove slide valve port. J. Harbin Univ. Sci. Technol. 29 (1). https://doi.org/10.15938/j.jhust.2024.01.004 (in Chinese).
Xie, Z., Wang, Y., Ni, J., Yin, J., Yu, D., Liu, J., 2023. Friction torque analysis of planetary roller screw based on the creepage theory. Tribol. Int. 178, 108059. https://doi.org/10.1016/j.triboint.2022.108059.
Xu, L.P., Ma, H.Y., Ren, D.Z., 2019. Numerical simulation for multi-way valves and fit clearance research based on heat-fluid-solid coupling. J. Eng. 2019 (13), 247–252. https://doi.org/10.1049/joe.2018.9036.
Xu, N., Zhang, S.M., Jia, D.L., Chen, Q., Yao, B.C., 2024. Effect of spool posture on control valve performance considering outlet shape and large fit clearance. Geoenergy Sci. Eng. 232, 212453. https://doi.org/10.1016/j.geoen.2023.212453.
Ye, Y., Yin, C.B., Li, X.D., Zhou, W.J., Yuan, F.F., 2014. Effects of groove shape of notch on the flow characteristics of spool valve. Energy Convers. Manag. 86, 1091–1101. https://doi.org/10.1016/j.enconman.2014.06.081.
Yin, F.L., Chen, Y.T., Ma, Z.H., Nie, S.L., Ji, H., 2023. Investigation on mixed thermalelstohydrodynamic lubrication behavior of slipper/swash plate interface in water hydraulic axial piston pump. Tribol. Int. 189, 108896. https://doi.org/10.1016/j.triboint.2023.108896.
You, Y., Wang, S., Lv, W., Chen, Y., Gross, U., 2021. A CFD model of frost formation based on dynamic meshes technique via secondary development of ANSYS fluent. Int. J. Heat Fluid Flow 89, 108807. https://doi.org/10.1016/j.ijheatfluidflow.2021.108807.
Yu, R.M., Ma, Y.Y., Liu, K.L., Liu, X.Y., 2024. Study on the design of single-seat control valve with stable flow regulation and its fluid flow characteristics and thermal stress. Flow Meas. Instrum. 95, 102486. https://doi.org/10.1016/j.flowmeasinst.2023.102486.
Zhang, J.H., Lyu, F., Xu, B., Huang, W.D., Wu, W., Guo, Z.M., Xu, H.G., Huang, X.C., 2021. Simulation and experimental investigation on low wear rate surface contour of piston/cylinder pair in an axial piston pump. Tribol. Int. 162, 107127. https://doi.org/10.1016/j.triboint.2021.107127.
Zhang, X.B., Xie, Y.D., Han, J.Z., Wang, Y., 2022. Design of control valve with low energy consumption based on isight platform. Energy 239, 122328. https://doi.org/10.1016/j.energy.2021.122328.
Zhang, Y., Wang, S.P., Shi, J., Wang, X., 2020. Evaluation of thermal effects on temperature-sensitive operating force of flow servo valve for fuel metering unit. Chin. J. Aeronaut. 33 (6), 1812–1823. https://doi.org/10.1016/j.cja.2019.09.011.
Zhao, J.Y., Qiu, B.J., Man, J.X., 2020. A piston-swiveling-cylinder pair in a high water-based hydraulic motor with self-balanced distribution valves. Energies 13 (12), 3175. https://doi.org/10.3390/en13123175.
Zhao, S.D., Liu, Y.S., Wu, D.F., Wang, C.M., Wang, Z.Y., 2023. Theoretical and experimental flow characteristics of a large-scale annular channel in terms of deformation gradient, eccentricity, and water compressibility. Lubricants 11 (3), 134. https://doi.org/10.3390/lubricants11030134.
Zhao, X.L., Liu, Y.L., 2020. Research progress and prospect of intelligent separate injection technology for water injection wells. Pet. Geol. Eng. 34 (4), 123–126. https://doi.org/10.3969/j.issn.1673-8217.2020.04.025 (in Chinese).

Zheng, X.Q., Shi, J.F., Cao, G., Yang, N.Y., Cui, M.Y., Jia, D.L., Liu, H., 2022. Progress and prospects of oil and gas production engineering technology in China. Petrol. Explor. Dev. 49 (3), 644–659. https://doi.org/10.1016/S1876-3804(22)60054-5.

Zhu, Y., Yang, Y., Lu, P., Ge, X., Yang, H., 2019. Influence of surface pores on selective laser melted parts under lubricated contacts: A case study of a hydraulic spool valve. Virtual Phys. Prototyp. 14 (4), 395–408. https://doi.org/10.1080/17452759.2019.1633930.